2003

Inversion-based output tracking control and learning control for nonminimum phase systems and RF CMOS LNA and mixer design

Xuezhen Wang
Iowa State University

Inversion-based output tracking control and learning control for nonminimum phase systems and RF CMOS LNA and mixer design

by

Xuezhen Wang

A dissertation submitted to the graduate faculty
in partial fulfillment of the requirements for the degree of
DOCTOR OF PHILOSOPHY

Major: Electrical Engineering (Microelectronics)

Program of Study Committee:
Degang Chen, Co-major Professor
Robert Weber, Co-major Professor
Murti Salapaka
Julie Dickerson
Ping Lu

Iowa State University
Ames, Iowa
2003

Graduate College
Iowa State University

This is to certify that the Doctoral dissertation of

Xuezhen Wang

has met the dissertation requirements of Iowa State University

Signature was redacted for privacy.

Co-major Professor

Signature was redacted for privacy.

Co-major Professor

Signature was redacted for privacy.

For the Major Program

DEDICATION

To my family and friends who love me and whom I love

TABLE OF CONTENTS

LIST OF TABLES

LIST OF FIGURES

ACKNOWLEDGMENTS

Special thanks to my major professor Dr. Degang Chen for his intelligent guidance, unlimited support, and his unfailing encouragement. I would like to thank him for his financial support for my study and research at Iowa State University.

Thanks to my co-major professor Dr. Weber Robert for his supervision. His unique perspective of microwave and circuit theory and his rich industrial experience enhanced my understanding of many fundamental problems in microwave and circuit theory. His advice has always been appreciated and valued by me.

I would also like to thank the following Professors Dr. Murti V. Salapaka, Dr. Ping Lu, and Dr. Julie Dickson for serving on my graduate committee. I greatly appreciate their valuable comments and suggestions on this work.

My sincere thanks to Vincent Van Acker and Felicidade Van Acker for their precious help, friendship, understanding, and encouragement. Thanks to Maribel Kraybill for constant encouragement. Thanks to Mark Mehl for proofreading that improved the clarity of the dissertation. I would also like to thank Wei Wang for his frank encouragement and help.

Many thanks to Jeff N. Eisenbeis for his sincere encouragement, help, and many useful discussions. Thanks to Jialing Liu for his help, valuable discussions, and helpful suggestions. Thanks Jinghua Jin for her encouragement and help.

I would like to thank Abu Sebastian, Deepak R. Sahoo, Hullas Sehgal, Tathagata De, Vikas Yadav, and Muhammad J. Khan for their help. I would like to express my thanks and appreciation to all others who helped both with my dissertation and with any other aspects of education.

Last, but foremost, my special thanks go to my family for their patience, encourage-

ment, fully understanding, and unfailing love and affection during all these years.

This research was partially supported by the National Science Foundation under Grant No. ECS-9810398. They are much appreciated.

ABSTRACT

This thesis is composed of two parts. The first part of the thesis focuses on studying inversion-based output tracking control and learning control for nonminimum phase systems. The second part of the thesis focuses on RF CMOS LNA and mixer design.

The nonminimum phase property has long been recognized as a major obstacle in many control problems. In part one, we introduce a new design procedure for output tracking control of nonminimum phase systems. We provide a causal inversion solution for general nonlinear systems. By using the scaling property, we present a causal inversion solution such that the causal state and input trajectories track those obtained by stable inversion approach for linear systems. This new controller achieves stable ϵ—tracking. In contrast to stable inversion, the causal inversion approach does not require precalculation. In contrast to nonlinear regulation, the causal inversion approach avoids the numerical intractability of solving nonlinear PDEs. As an example of the application, a causal inversion-based controller is designed for tip trajectory tracking of a one-link flexible manipulator. Inversion-based adaptive and robust learning algorithms are developed for unstable nonminimum phase systems.

Fast growth of personal communication market puts a high demand on the production of low cost and low power transceivers for wireless applications. In part two, we present a design of a CMOS low noise amplifier and does its sensitivity analysis which is beneficial for making appropriate design trade offs. We also propose a novel low voltage down-conversion mixer design. As an example, all the circuits have been designed at 5.8 GHz and integrated in a TSMC 0.18 μm CMOS process. These front-end circuit designs can be used for low voltage and low power wireless applications.

1 INTRODUCTION

This thesis is composed of two parts. The first part of the thesis focuses on studying inversion-based output tracking control and learning control for nonminimum phase systems. The second part of the thesis studies RF CMOS LNA and mixer design.

In part one, we introduce a new design procedure for output tracking control of nonminimum phase systems. This new controller achieves stable $\epsilon-$tracking. In contrast to stable inversion, the causal inversion approach does not require precalculation. In contrast to nonlinear regulation, the causal inversion approach avoids the numerical intractability of solving nonlinear PDEs. As an example of the application, a causal inversion-based controller is designed for tip trajectory tracking of a one-link flexible manipulator. Inversion-based adaptive and robust learning algorithms are developed for unstable nonminimum phase systems. This research is useful for applications with nonminimum phase property.

In part two, we present a design of a CMOS low noise amplifier and does its sensitivity analysis which is beneficial for making appropriate design trade offs. We also propose a novel low voltage down-conversion mixer design. As an example, all the circuits have been designed at 5.8 GHz and integrated in a TSMC 0.18 μm CMOS process. These front-end circuit designs can be used for low voltage and low power wireless applications.

The remainder of this chapter is organized as follows. Section 1.1 describes the motivation for studying the inversion-based output tracking control and learning control for nonminimum phase systems and RF CMOS LNA and mixer design. Section 1.2 describes the outline of the thesis.

1.1 Motivation

Output tracking control of nonminimum phase systems is a highly challenging problem encountered in many practical engineering applications. The nonminimum phase property has long been recognized as a major obstacle in many control problems. The solution of the nonlinear regulator involves solving a set of nonlinear PDEs. At the same time, the transient errors cannot be controlled precisely and can be large, in general, for nonminimum phase systems. Output tracking control using a stable inversion approach obtains both bounded state and input trajectories. However, the drawback is that stable inversion is noncausal. For this reason, we consider a new method to solve the output tracking control of nonminimum phase systems.

Iterative learning control (ILC) is a feed forward control approach aimed at achieving high performance output tracking control by "learning" from past experience so as to eliminate the repetitive errors from future execution. Although the existing learning algorithms have been theoretically proven to provide output error convergence and have had successful applications, many such algorithms have practical difficulties with nonminimum phase systems, especially for the unstable nonminimum phase systems with unknown parameters and uncertainties. This motivates us to develop an adaptive and robust learning algorithm working for unstable nonminimum phase systems.

Wireless communications research has experienced a remarkable renaissance in the last decade. Fast growth of personal communication market places a high demand on the production of low cost and low power transceivers for wireless applications. As a low cost alternative, CMOS is becoming a contender for RF front-end IC applications. However, there are fewer examples of low voltage and low power CMOS low noise amplifier (LNA) designed. At the same time, in low-voltage RF IC design, high LO drives are difficult to generate. The most common mixer architecture cannot operate at near 1 V supply due to the stack of the three saturated transistors. Thus designing a CMOS mixer with low voltage becomes a challenging task. All these challenging targets motivate us to design a low voltage and low power front-end RF CMOS LNA and mixer.

Each chapter is a self-contained paper which has been published in peer-reviewed

conferences or has been submitted to peer-reviewed journals or conferences and are still in the reviewing process.

1.2 Thesis Outline

This thesis is organized as follows. Part one contains chapter 2 to chapter 4. Part two includes chapter 5 and chapter 6.

Chapter 2 This chapter introduces a new design procedure for output tracking control of nonminimum phase systems. This new controller achieves stable $\epsilon-$tracking of a reference profile given in real time via a causal inversion approach. In this approach, the nonminimum phase system is first stably inverted on-line to obtain both desired (and stable) state and input trajectories. Then an H_∞ optimal controller is used to stabilize the closed-loop system. We provide a causal inversion solution for general nonlinear systems. By using the scaling property, we present a causal inversion solution such that the causal state and input trajectories track those obtained by stable inversion approach for linear systems. In contrast to stable inversion, the causal inversion approach does not require precalculation. In contrast to nonlinear regulation, the causal inversion approach avoids the numerical intractability of solving nonlinear PDEs. As an example of the application, a causal inversion-based controller is designed for tip trajectory tracking of a one-link flexible manipulator. Simulation results demonstrate its effectiveness in output tracking. This whole manuscript has been submitted to IEEE Transactions on Control System Technology for peer review. With positive review comments, the revised version has been submitted for the further review. Part of the results has been published in several peer-reviewed conferences, which are *2001 40st IEEE Conference on Decision and Control, 2002 45th Midwest Symposium on Circuits and Systems, and Proceedings of the 2002 International Conference on Control Applications.*

Chapter 3 In this chapter, a new adaptive learning algorithm is presented for the

repetitive tracking control of a class of unstable nonminimum phase systems. After each repetitive trial, a Least-Squares method is used to estimate the system parameters. The output tracking error and the identified system model are used through stable inversion to find the feed forward input, together with the desired state trajectories, for the next trial. An adaptive backstepping based tracking controller is used in each trial to ensure the regulation of the desired state trajectories. Simulation results demonstrate that the proposed learning control scheme is very effective in reproducing the desired trajectories. This whole manuscript has been published in the peer-reviewed conference, The *2000 IEEE International Conference on Systems, Man and Cybernetics.*

Chapter 4 This chapter introduces a new robust inversion-based learning algorithm for the repetitive tracking control of a class of unstable nonminimum phase systems. After each repetitive trial, the Least-Squares method is used to estimate the system parameters. The output tracking error and the identified system model are used through stable inversion to find the feed forward input, together with the desired state trajectories, for the next trial. A robust controller is used in each trial to ensure the stability of the systems and the output tracking error convergence. Sufficient conditions for learning control convergence are provided. Simulation studies on systems with gain uncertainty and time constant uncertainty are also presented. In addition, simulation results demonstrate that the proposed learning control scheme is very effective in reproducing the desired trajectories. This whole manuscript has been submitted to IEE Proceedings of Control Theory and Applications for peer review. Part of the results has been published in the peer-reviewed conference, The *2002 IEEE International Conference on Systems, Man and Cybernetics.*

Chapter 5 This chapter presents a 5.8 GHz low voltage and low power LNA design integrated in a TSMC 0.18 μm CMOS process, and its sensitivity analysis. This sensitivity analysis gives a measure of the sensitivity of the LNA performance to

a change in the circuit element values, thereby assisting the designer to choose adequate circuit-element tolerances. Such sensitivity analysis of the LNA is very beneficial for making appropriate design trade offs. The method employed here is inductive source degeneration. All the spiral inductors are implemented on-chip. This whole manuscript has been published in the peer-reviewed conference, *NASA Symposium on VLSI Circuit Design.*

Chapter 6 This paper presents a 5.8 GHz low voltage down-conversion mixer design integrated in a TSMC 0.18 μm CMOS process. The proposed method features an RF input stage that converts the RF input voltage to current, which is coupled to the core of a Gilbert Cell using current mirrors. This implementation eliminates the current source transistor at the bottom and furthermore reduces the supply voltage. Common-mode feedback is used for the active load of the mixer. The LO frequency is at 5.6 GHz. The designed mixer requires only a 1.5 V supply voltage. This whole manuscript has been submitted to 2004 IEEE International Symposium on Circuits and Systems for peer review. Part of the results has been published in the peer-reviewed conference, the *2003 IEEE Radio and Wireless Conference.*

Chapter 7 finally gives the conclusions. It summarizes the contributions presented in this thesis and also provides some possible future research directions for the further improvement and extended study.

2 Output Tracking Control of a One-Link Flexible Manipulator via Causal Inversion

Abstract — Output tracking control is a challenging problem. This paper introduces a new design procedure for output tracking control of nonminimum phase systems. This new controller achieves stable $\epsilon-$tracking of a reference profile given in real time via a causal inversion approach. In this approach, the nonminimum phase system is first stably inverted on-line to obtain both desired (and stable) state and input trajectories. Then an H_∞ optimal controller is used to stabilize the closed-loop system. In contrast to stable inversion, the causal inversion approach does not require precalculation. In contrast to nonlinear regulation, the causal inversion approach avoids the numerical intractability of solving nonlinear PDEs. As an example of the application, a causal inversion-based controller is designed for tip trajectory tracking of a one-link flexible manipulator. Simulation results demonstrate its effectiveness in output tracking.

2.1 Introduction

A system is nonminimum phase (or has unstable zeros in the linear case) if a nonlinear state feedback can hold the system output identically zero while the internal dynamics become unstable [7]. Output tracking control of nonminimum phase systems is a highly challenging problem encountered in many practical engineering applications. The nonminimum phase property has long been recognized as a major obstacle in many control problems. It is well known that unstable zeros cannot be moved with state feedback; whereas, if completely controllable [13], the poles can be arbitrarily placed.

The classical inversion approach for output tracking control uses stabilizing feedback

together with feed-forward signals generated by an inverse system. The classical inverse problem was first studied by Brockett and Mesarovic [1]. In Silverman's procedure [11], an input function defined on $[0, \infty)$ is obtained by solving an initial condition problem for a given output function. Such inverses can be causal but unstable for nonminimum phase systems. These linear results were extended to nonlinear real-analytical systems by Hirschorn [6] and Singh [12]. Similar to the linear cases, these inversion algorithms produce causal inverses for a given desired output $y_d(t)$ and a fixed initial condition $x(t_0)$, leading to unbounded $u(t)$ and $x(t)$ for nonminimum phase systems.

The nonlinear regulation technique for output tracking control was first developed by Isidori and Byrnes [8]. This theory provides asymptotic output tracking of reference signals generated by an exosystem for a class of nonlinear systems with guaranteed internal stability. The solution of the nonlinear regulator involves solving a set of nonlinear PDEs. At the same time, the transient errors cannot be controlled precisely and can be large, in general, for nonminimum phase systems.

The stable inversion approach was first provided by Chen and Paden [2]. It was then applied to the nonlinear control problem: output tracking control of nonminimum phase systems [4, 5]. The output tracking controller in [4, 5] has a feed-forward structure with feedback. Both bounded state and input trajectories are obtained. However, the drawback is that stable inversion is noncausal.

This paper introduces a new procedure for designing an output tracking controller for nonminimum phase systems of a causal reference trajectory. This new controller achieves stable $\epsilon-$tracking, using a novel approach derived from causal inversion. In this approach, the nonminimum phase system is first stably inverted on-line to obtain both desired (and stable) state and input trajectories. Then an H_∞ optimal controller is used to stabilize the closed-loop system. Compared to the stable inversion method, the causal inversion approach does not require precalculation. Compared to the nonlinear regulation method, causal inversion avoids the numerical intractability of solving nonlinear PDEs and transient errors are relatively small. As an example, a causal inversion-based controller is designed for a one-link flexible manipulator system, in which preloading the

links is not required.

The remainder of this paper is organized as follows. The next section defines the basic framework and the problem to be solved. Section 2.3 defines the causal inversion problem and presents the solution with its properties for a class of systems. Section 2.4 studies the controller design problem. Section 2.5 applies the causal inversion approach to design a tip trajectory tracking controller for a one-link flexible manipulator. Simulation results are discussed. Finally, concluding remarks are given in Section 2.6.

2.2 Basic Framework

Consider a nonlinear system of the form

$$\begin{cases} \dot{x} = f(x) + g(x)u \\ y = h(x) \end{cases} \tag{2.1}$$

defined on a neighborhood X of the origin in $\Re^n$, with input $u \in \Re^m$ and output $y \in \Re^p$. $f(x)$ and $g_i(x)$ (the i^{th} column of $g(x)$) for $i = 1, 2, \cdots, m$ are smooth vector fields, and $h_i(x)$ for $i = 1, 2, \cdots, p$ are smooth functions on X, with $f(0) = 0$ and $h(0) = 0$.

Without loss of generality (WLOG), consider a nonlinear system of the form (2.1) with the same number m of inputs and outputs and

$$\begin{aligned} y &= (y_1, y_2, \cdots, y_m)^T \\ u &= (u_1, u_2, \cdots, u_m)^T \\ h(x) &= [h_1(x), h_2(x), \cdots, h_m(x)]^T \\ g(x) &= [g_1(x), g_2(x), \cdots, g_m(x)]. \end{aligned}$$

Making the following assumptions:

A1 : This system (2.1) has a well-defined relative degree $r = \{r_1, r_2, \cdots, r_m\}^T \in N^m$ at the equilibrium point $x = 0$; that is, in an open neighborhood of $x = 0$,
(i) for all $1 \leq j \leq m$, for all $1 \leq i \leq m$, for all $k < r_i - 1$ and $k \geq 0$, and for all x,

$$L_{g_j} L_f^k h_i(x) = 0, \tag{2.2}$$

(ii) the $m \times m$ matrix $\beta(x)$ with $\beta_{ij}(x) \triangleq L_{g_j} L_f^{(r_i - 1)} h_i(x)$ is nonsingular.

Note that since the control u does not appear explicitly in $y = h(x)$, it yields $r_i \geq 1$ for all i. Therefore, $r_i - 1 \in N$ and the operation in the definition of β is well defined [3].

A2 : The reference output trajectory $y_d(t)$ is a sufficiently smooth function of time. $y_d(t), \dot{y}_d(t), \cdots, y_d^{(r-1)}, y_d^{(r)} \in L_1 \cap L_\infty$, with $y_d(t) \equiv 0$ for $t = 0$.

A3 : The system (2.1) is stabilizable and observable.

For a given reference $y_d(t)$ satisfying Assumption A2, the following tracking problem is defined:

Definition 1 : The system is said to achieve *stable asymptotic-tracking* if $\|y_d(t) - y(t)\| \to 0$, as $t \to \infty$ with bounded $x(t)$ and $u(t)$.

Remark : Under A2, Definition 1 appears automatically satisfied as long as the closed-loop system is stabilized. However, if $y_d(t)$ has a nonzero final value as mentioned in the previous remark, the tracking problem requires much more than stabilization.

Definition 2 : Given an $\epsilon > 0$, the system is said to achieve *Stable $\epsilon-$Tracking* if $\|y_d(\cdot) - y(\cdot)\|_{L_2} < \epsilon$ with bounded $x(t)$ and $u(t)$.

Note that stable $\epsilon-$tracking implies stable asymptotic-tracking. The proposed controller will provide a stable $\epsilon-$tracking for nonminimum phase systems of a causal reference trajectory.

2.3 Causal Inversion Problems

For the system (2.1), consider the following problem [14]:

Causal Inversion Problem: Given $y_d(t)$ satisfying Assumption A2, find a nominal control input $\bar{u}_d(t)$ and a desired state trajectory $\bar{x}_d(t)$ such that

(1) $\bar{u}_d$ and $\bar{x}_d$ are bounded, and

$$\bar{u}_d(t) \to 0, \quad \bar{x}_d(t) \to 0, \quad \text{as} \quad t \to \infty.$$

(2) $\bar{x}_d(t)$ and $\bar{u}_d(t)$ are causal; that is, $\bar{x}_d(t) \equiv 0, \bar{u}_d(t) \equiv 0$ for $t \leq 0$.

(3) Exact output matching is achieved

$$h(\bar{x}_d(t)) = y_d(t) \tag{2.3}$$

and

$$L_f^i h(\bar{x}_d) = y_d^{(i)}, \text{ for } i = 1, \cdots, r_i - 1. \tag{2.4}$$

(4) $\dot{\bar{x}}_d - f(\bar{x}_d) - g(\bar{x}_d)\bar{u}_d \to 0$ as $t \to \infty$.

Remark : In the stable inversion problem, condition (2) is not required and it requires

$$\dot{x}_d = f(x_d) + g(x_d)u_d,$$

where x_d and u_d are the unique solution to the stable inversion problem. This difference implies that the stable inversion solution is required to satisfy the system dynamics for all time but the new causal inversion solution is only required to satisfy the system dynamics asymptotically. As a result, the causal inverse solution $\bar{u}_d$, if applied as the sole input to the system in an open-loop fashion, will not be able to generate y_d exactly. In contrast, the stable inverse solution u_d is capable of generating y_d exactly in the ideal case. However, as it will become clear later, the causal inverse solution does approximately track the stable inverse solution with the added property of being causal. The word "inversion" in our causal inversion implies that $\bar{x}_d$ does provide exact output matching; that is,

$$h(\bar{x}_d(t)) = y_d(t),$$

and

$$L_f^i h(\bar{x}_d) = y_d^{(i)}, \text{ for } i = 1, \cdots, r_i - 1.$$

This is very appealing since one almost never implements an inverse control in open-loop. In contrast, with this approach, a stabilizing feedback control can be designed to track $\bar{x}_d(t)$ which leads to tracking of $y_d(t)$. We will design such controllers in Section 2.4.

2.3.1 Causal Inversion for Nonlinear Systems

From Assumption A2, "certain" is made clear here, which means y_d should be r times differentiable. Under Assumption A1, the system can be partially linearized. To do this, y_i is differentiated until at least one u_i appears explicitly. This will happen at exactly the r_i-th derivative of y_i due to (2.2). Define $\xi_k^i = y_i^{(k-1)}$ for $i = 1, \cdots, m$ and

$k = 1, \cdots, r_i$, and denote

$$\begin{aligned}\xi &= (\xi_1^1, \xi_2^1, \cdots, \xi_{r_1}^1, \xi_1^2, \cdots, \xi_{r_2}^2, \cdots, \xi_{r_m}^m)^T \\ &= (y_1, \dot{y}_1, \cdots, y_1^{(r_1-1)}, y_2, \cdots, y_2^{(r_2-1)}, \cdots, y_m^{(r_m-1)})^T.\end{aligned}$$

Choose η, an $n - \sum r_i$ dimensional function on $\Re^n$, such that $(\xi^T, \eta^T)^T = \psi(x)$ forms a change of coordinate with $\psi(0) = 0$ [7]. In this new coordinate system, the system dynamics of (2.1) becomes

$$\begin{cases} \dot{\xi}_1^i = \xi_2^i \\ \vdots \\ \dot{\xi}_{r_i-1}^i = \xi_{r_i}^i \\ \dot{\xi}_{r_i}^i = \alpha_i(\xi, \eta) + \beta_i(\xi, \eta)u \end{cases} \quad \text{for} \quad i = 1, \cdots, m \tag{2.5}$$

$$\dot{\eta} = q_1(\xi, \eta) + q_2(\xi, \eta)u,$$

which, in a more compact form, is equivalent to

$$y^{(r)} = \alpha(\xi, \eta) + \beta(\xi, \eta)u \tag{2.6}$$

$$\dot{\eta} = q_1(\xi, \eta) + q_2(\xi, \eta)u, \tag{2.7}$$

where

$$\begin{aligned} y^{(r)} &= [y_1^{(r_1)}, y_2^{(r_2)}, \cdots, y_m^{(r_m)}]^T \\ \alpha(\xi, \eta) &= [\alpha_1(\xi, \eta), \alpha_2(\xi, \eta), \cdots, \alpha_m(\xi, \eta)]^T \\ \beta(\xi, \eta) &= [\beta_1^T(\xi, \eta), \beta_2^T(\xi, \eta), \cdots, \beta_m^T(\xi, \eta)]^T, \end{aligned}$$

and $\alpha(0, 0) = 0$ since $f(0) = 0$. By the relative degree assumption, $\beta(\xi, \eta)$ is nonsingular, and the following feedback control law

$$u \triangleq \beta^{-1}(\xi, \eta)[v - \alpha(\xi, \eta)] \tag{2.8}$$

is well defined and partially linearizes the input-output dynamics relationship into m chains of integrators, $y_i^{(r_i)} = v_i$, for $i = 1, 2, \cdots, m$; where $v = [v_1, v_2, \cdots, v_m]^T \in \Re^m$ is the new control input. The inversion problem requires $y(t) \equiv y_d(t)$, which leads to:

$$v_i = y_{d_i}^{(r_i)}, \quad i = 1, 2, \cdots, m$$

$$\xi = \xi_d \triangleq (y_{d_1}, \dot{y}_{d_1}, \cdots, y_{d_1}^{(r_1-1)}, y_{d_2}, \cdots, y_{d_2}^{(r_2-1)}, \cdots, y_{d_m}^{r_m-1})^T. \tag{2.9}$$

Equation (2.7) becomes the zero dynamics driven by the reference output trajectory,

$$\dot{\eta} = p(y_d^{(r)}, \xi_d, \eta), \tag{2.10}$$

where

$$\begin{aligned} y_d^{(r)} &= [y_{d_1}^{(r_1)}, y_{d_2}^{(r_2)}, \cdots, y_{d_m}^{(r_m)}]^T \\ p(y_d^{(r)}, \xi_d, \eta) &= q_1(\xi_d, \eta) + q_2(\xi_d, \eta)[\beta(\xi_d, \eta)]^{-1}[y_d^{(r)} - \alpha(\xi_d, \eta)]. \end{aligned}$$

Equation (2.10) is often called the reference dynamics.

A4 : $\eta = 0$ is a hyperbolic equilibrium point of the reference zero dynamics.

Linearizing the right hand side of (2.10) at the equilibrium point $\eta = 0$ gives

$$\dot{\eta} = A\eta + By_d^{(r)} + g(t), \tag{2.11}$$

where

$$\begin{aligned} A &= \frac{\partial p}{\partial \eta}(y_d^{(r)}, \xi_d, \eta)|_{\eta=0,\, \xi_d=0,\, y_d^{(r)}=0} \\ B &= \frac{\partial p}{\partial y_d^{(r)}}(y_d^{(r)}, \xi_d, \eta)|_{\eta=0,\, \xi_d=0,\, y_d^{(r)}=0} \\ g(t) &= p(y_d^{(r)}, \xi_d, \eta) - A\eta - By_d^{(r)}. \end{aligned}$$

For a real matrix A, there exists an invertible $(n - \sum r_i) \times (n - \sum r_i)$ matrix P_1, such that $\bar{J} = P_1^{-1}AP_1$, where $\bar{J}$ is the real Jordan form of A. Therefore, with the coordinate transformation $\eta = P_1[\eta_s \quad \eta_u]^T$, the reference dynamics in the new coordinate is in real Jordan form. As a result, (2.10) can be rewritten as:

$$\dot{\eta}_s = A_s\eta_s + B_s y_d^{(r)} + d_s(y_d^{(r)}, \xi_d, \eta_s, \eta_u), \quad \eta_s(\pm\infty) = 0 \tag{2.12}$$

$$\dot{\eta}_u = A_u\eta_u + B_u y_d^{(r)} + d_u(y_d^{(r)}, \xi_d, \eta_s, \eta_u), \quad \eta_u(\pm\infty) = 0, \tag{2.13}$$

where

$$\bar{J} = P_1^{-1}AP_1 = \begin{bmatrix} A_s & 0 \\ 0 & A_u \end{bmatrix}, \quad \begin{bmatrix} B_s \\ B_u \end{bmatrix} = P_1 B,$$

and A_s has all eigenvalues in the open left-half plane with dimension $n_s \times n_s$, A_u has all eigenvalues in the open right-half plane with dimension $n_u \times n_u$, B_s is with dimension

$n_s \times 1, B_u$ is with dimension $n_u \times 1$, and $d_s(\cdot)$ and $d_u(\cdot)$ denote the higher order terms (H.O.T.) of the expression.

Together with (2.9), these define the desired stable inverse system, from which a bounded but noncausal inverse solution can be obtained [3].

For the causal inversion problem, a controller $\bar{v}$ is introduced to stabilize the unstable reference zero dynamics. Two dynamic equations yield the following:

$$\dot{\bar{\eta}}_s = A_s\bar{\eta}_s + B_s y_d^{(r)} + d_s(y_d^{(r)}, \bar{\xi}_d, \bar{\eta}_s, \bar{\eta}_u), \quad \bar{\eta}_s(0) = 0 \tag{2.14}$$

$$\dot{\bar{\eta}}_u = A_u\bar{\eta}_u + B_u y_d^{(r)} + d_u(y_d^{(r)}, \bar{\xi}_d, \bar{\eta}_s, \bar{\eta}_u) + \bar{v}, \quad \bar{\eta}_u(0) = 0, \tag{2.15}$$

where $\bar{\xi}_d = \xi_d$, and $\bar{v}$ is to be chosen to reach the asymptotic stability of (2.14, 2.15). By selecting

$$\bar{v} = -kA_u\bar{\eta}_u - kB_u y_d^r - kd_u(y_d^{(r)}, \bar{\xi}_d, \bar{\eta}_s, \bar{\eta}_u), \tag{2.16}$$

where $k \geq 2$, then equation (2.15) becomes

$$\dot{\bar{\eta}}_u = -(k-1)A_u\bar{\eta}_u - (k-1)B_u y_d^{(r)} - (k-1)d_u(y_d^{(r)}, \bar{\xi}_d, \bar{\eta}_s, \bar{\eta}_u), \quad \bar{\eta}_u(0) = 0. \tag{2.17}$$

Note that $-A_u$ is Hurwitz and $d_u(\cdot)$ in (2.17) is H.O.T. By Assumption A2, $y_d^{(i)} \to 0$, for $i = 1, \cdots, r$ as $t \to \infty$. Notice that $\bar{\eta} = 0$ is an exponentially stable equilibrium point for the nonlinear system (2.17) [9]. Hence $\bar{\eta}_u(t) \to 0$ as $t \to \infty$ is obtained. Plugging $\bar{\eta}_u$ into (2.14), and regarding it as an external input, the same argument leads to $\bar{\eta}_s(t) \to 0$ as $t \to \infty$. Thus $\bar{\eta}(t) \to 0$ as $t \to \infty$. Also, $\bar{\xi}_d \to 0$ as $t \to \infty$. Therefore, there exist a constant $T > 0$ such that $\|\bar{\xi}_d(t)\|_{L_2}$ and $\|\bar{\eta}(t)\|_{L_2}$ are inside a closed ball with radius ϵ when $t > T$, where $\epsilon > 0$. On the closed ball, $\psi(\bar{x}_d) = [\bar{\xi}_d^T \quad \bar{\eta}^T]^T = [\bar{\xi}^T, \quad [\bar{\eta}_s^T \quad \bar{\eta}_u^T]P_1^T]^T$ defines a local diffeomorphism. Its inverse

$$\bar{x}_d = \phi(\bar{\xi}_d, \bar{\eta}) \tag{2.18}$$

is a smooth mapping, that is, it has continuous partial derivatives of any order. Therefore, there exists a constant L, such that $\|D\phi\| \leq L$.

From the definition of y_d and (2.9, 2.14, 2.17), we can have $\dot{\bar{\xi}}_d(t), \dot{\bar{\eta}}_s(t), \dot{\bar{\eta}}_u(t) \to 0$ as $t \to \infty$. It yields $\dot{\bar{\eta}}(t) \to 0$ as $t \to \infty$. It further produces

$$\|\bar{\xi}_d\|_{L_2} \leq \epsilon \tag{2.19}$$

$$\|\bar{\eta}_d\|_{L_2} \leq \epsilon \tag{2.20}$$

where $\epsilon > 0$. From (2.18), we have

$$\dot{\bar{x}}_d = D\phi[\dot{\bar{\xi}}_d, \dot{\bar{\eta}}]^T. \tag{2.21}$$

Consequently, it yields

$$\|\dot{\bar{x}}_d\|_{L_2} \leq \|D\phi\|_{L2}\|[\dot{\bar{\xi}}_d, \dot{\bar{\eta}}]\|^T \leq L\|[\dot{\bar{\xi}}_d, \dot{\bar{\eta}}]\|^T. \tag{2.22}$$

From (2.19, 2.20), we have

$$\|\dot{\bar{x}}_d\|_{L_2} \to 0, \text{ as } t \to \infty. \tag{2.23}$$

Therefore,

$$\dot{\bar{x}}_d \to 0, \text{ as } t \to \infty. \tag{2.24}$$

Meanwhile,

$$\bar{u}_d = \beta^{-1}(\bar{\xi}_d, \bar{\eta})[y_d^{(r)} - \alpha(\bar{\xi}_d, \bar{\eta})]. \tag{2.25}$$

Then $\bar{x}_d$ and $\bar{u}_d$ are bounded and $\bar{x}_d(t), \bar{u}_d(t) \to 0$ as $t \to \infty$. Moreover, by the definition of $\bar{\xi}_d$, $h(\bar{x}_d) = y_d$ and $L_f^i h(\bar{x}_d) = y_d^{(i)}$ for $i, \cdots, r_i - 1$ are obtained. At the same time, since $\bar{x}_d(t), \bar{u}_d(t) \to 0$ as $t \to \infty$, then

$$f(\bar{x}_d) + g(\bar{x}_d)\bar{u}_d \to 0, \text{ as } t \to \infty. \tag{2.26}$$

Combining (2.24,2.26) yields

$$\dot{x}_d - f(\bar{x}_d) - g(\bar{x}_d)\bar{u}_d \to 0, \text{ as } t \to \infty. \tag{2.27}$$

Thus a casual inversion solution to nonlinear systems has been provided. The algorithm can be summarized in the following theorem.

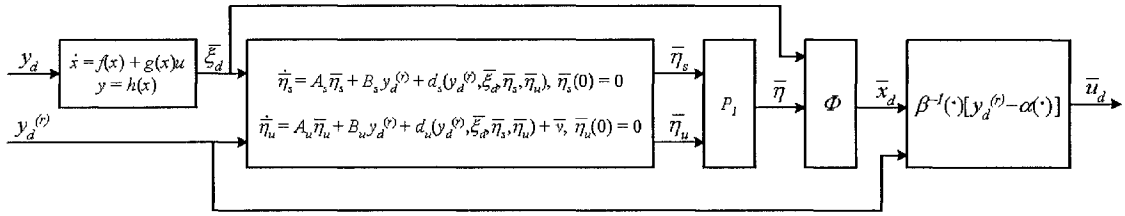

Figure 2.1 Block diagram of causal inversion

Theorem 1 : *Under Assumptions A1-A4, a causal inversion is given by (2.18, 2.25), where* $\bar{\xi}_d, \bar{\eta}_s$, *and* $\bar{\eta}_u$ *are solved by (2.9), (2.14), and (2.15) respectively, and* $\bar{v}$ *is given by (2.16).*

Without loss of generality, for simplicity, let $k = 2$ for the rest of this paper. The block diagram of causal inversion is shown in Figure 2.1.

By applying the same strategy to linear systems in the next section, this presentation will show that a causal inversion solution is obtained.

2.3.2 Causal Inversion Solution for Linear Systems

Consider a linear system of the form

$$\begin{cases} \dot{x} = Ax + Bu \\ y = Cx, \end{cases} \tag{2.28}$$

where $x \in \Re^n$, input $u \in \Re^m$, output $y \in \Re^m, A \in \Re^{n\times n}, B \in \Re^{n\times m}$, and $C \in \Re^{m\times n}$, with a well-defined vector relative degree. Given a smooth reference output trajectory $y_d(t)$ with $y_d(t) \equiv 0$ for $t \leq 0$ and $t \geq t_f$, for the inversion problem, let $y \equiv y_d$ and $u = u_d$ in (2.28). Then this system becomes

$$\begin{cases} \dot{x} = Ax + Bu_d \\ y_d = Cx. \end{cases} \tag{2.29}$$

Differentiating $y_d(t)$ until u_d appears explicitly in the right-hand side, solving for u_d, and substituting into (2.29) yields

$$\dot{x}(t) = \bar{A}x(t) + \bar{B}y_d^{(r)}(t) \tag{2.30}$$

$$u_d(t) = \bar{C}x(t) + \bar{D}y_d^{(r)}(t), \tag{2.31}$$

where $\bar{A} \in \Re^{n\times n}, \bar{B} \in \Re^{n\times m}, \bar{C} \in \Re^{m\times n}, \bar{D} \in \Re$ and

$$\begin{aligned}
\bar{A} &= A - B(CA^{(r-1)}B)^{-1}CA^r \\
\bar{B} &= B(CA^{(r-1)}B)^{-1} \\
\bar{C} &= -(CA^{(r-1)}B)^{-1}CA^r \\
\bar{D} &= (CA^{(r-1)}B)^{-1}
\end{aligned}$$

Now performing a change of variables

$$x_d = Pz = P[\xi, \eta_s, \eta_u]^T, \tag{2.32}$$

gives

$$\dot{\xi} = A_c\xi + B_c y_d^{(r)} \tag{2.33}$$

$$\dot{\eta_s} = A_s\eta_s + B_s y_d^{(r)} \tag{2.34}$$

$$\dot{\eta_u} = A_u\eta_u + B_u y_d^{(r)} \tag{2.35}$$

$$u_d = [C_c \quad C_s \quad C_u][\xi \quad \eta_s \quad \eta_u]^T + \bar{D}y_d^{(r)}, \tag{2.36}$$

where $\eta_s \in \Re^{n_s}, \eta_u \in \Re^{n_u}$; A_c, A_s, A_u are real Jordan matrices of suitable dimensions; A_c has r eigenvalues at zero; A_s has all eigenvalues in the open left-half plane; and A_u has all eigenvalues in the open right-half plane. Thus the inverse system has been decoupled to center, stable, and unstable subsystems.

Picking the transformation matrix P so that the center subsystem is a simple chain of r integrators, solving for ξ, and imposing two boundary conditions on the stable and unstable subsystems yield

$$\xi = [y_d, \dot{y}_d, \cdots, y_d^{(r-1)}]^T \tag{2.37}$$

$$\dot{\eta}_s = A_s\eta_s + B_s y_d^{(r)}, \quad t \geq 0; \quad \eta_s(t) = 0, \quad \forall\, t \leq 0 \tag{2.38}$$

$$\dot{\eta}_u = A_u\eta_u + B_u y_d^{(r)}, \quad t \leq t_f; \quad \eta_u(t) = 0, \quad \forall\, t \geq t_f. \tag{2.39}$$

Along with (2.36), these equations define the desired stable inverse system. For stable inversion, the bounded solutions are found by integrating forward in time for the stable subsystem and integrating backward in time for the unstable subsystem. In this approach, an *a priori* knowledge about $y_d^{(r)}$ is required, which means that it is a noncausal solution.

Here, a controller $\bar{v}$ is introduced to stabilize the unstable subsystem

$$\dot{\bar{\eta}}_u = A_u\bar{\eta}_u + B_u y_d^{(r)} + \bar{v}, \quad \bar{\eta}_u(0) = 0. \tag{2.40}$$

Choosing

$$\bar{v} = -2A_u\bar{\eta}_u - 2B_u y_d^{(r)} \tag{2.41}$$

and substituting it into (2.40) along with (2.39) yields

$$\dot{\bar{\eta}}_u = -A_u\bar{\eta}_u - B_u y_d^{(r)}, \quad \bar{\eta}_u(0) = 0. \tag{2.42}$$

Since A_s and $-A_u$ are Hurwitz, this result leads to bounded solutions for $\bar{\eta}_s(t)$ and $\bar{\eta}_u(t)$. Letting $y_d^{(i)} \to 0$, for $i = 1, \cdots, r$ as $t \to \infty$, causes $\bar{\eta}_s(t) \to 0$ and $\bar{\eta}_u(t) \to 0$ as $t \to \infty$. Also, $\bar{\xi}_d = 0$ for $t \leq 0$ and for $t \geq t_f$.

Set $\bar{\xi}_d = \xi$ and $\bar{\eta}_s = \eta_s$, and let

$$\bar{x}_d = P[\bar{\xi}_d, \bar{\eta}_s, \bar{\eta}_u]^T \tag{2.43}$$

$$\bar{u}_d = C_c\bar{\xi}_d + C_s\bar{\eta}_s + C_u\bar{\eta}_u + \bar{D}y_d^{(r)}. \tag{2.44}$$

Then $\bar{x}_d$ and $\bar{u}_d$ are bounded, and $\bar{x}_d(t), \bar{u}_d(t) \to 0$ as $t \to \infty$. And by the definition of $\bar{\xi}_d$, $C\bar{x}_d = y_d$ and $L_f^i h(\bar{x}_d) = y_d^{(i)}$ for $i = 1, \cdots, r_i - 1$ are obtained.

Likewise, a similar argument may be applied to linear systems. Since $\bar{x}_d(t), \bar{u}_d(t) \to 0$ as $t \to \infty$, we have

$$A\bar{x}_d + B\bar{u}_d \to 0, \text{ as } t \to \infty. \tag{2.45}$$

From the definition of y_d and (2.37, 2.38, 2.42),we can have $\dot{\bar{\xi}}_d(t), \dot{\bar{\eta}}_s(t), \dot{\bar{\eta}}_u(t) \to 0$ as $t \to \infty$. From (2.43), we have

$$\dot{\bar{x}}_d = P[\dot{\bar{\xi}}_d, \dot{\bar{\eta}}_s, \dot{\bar{\eta}}_u]^T. \tag{2.46}$$

Thus we have

$$\dot{\bar{x}}_d \to 0, \text{ as } t \to \infty. \tag{2.47}$$

Combining (2.45, 2.47), we have

$$\dot{\bar{x}}_d - A\bar{x}_d - B\bar{u}_d \to 0, \text{ as } t \to \infty \tag{2.48}$$

Thus the causal solution for linear systems has been provided.

Let $\tilde{\eta} = \bar{\eta}_u - \eta_u$. Suppose the initial condition for (2.39) is η_{u0}, then

$$\dot{\tilde{\eta}}_u = A_u\tilde{\eta}_u + \bar{v}, \quad \tilde{\eta}_u(0) = -\eta_{u0}. \tag{2.49}$$

Theorem 2 : *Consider a linear system described by (2.28). Given a low pass signal* $g(t) \in L_1 \cap L_\infty$ *and* $y_d^{(r)}(t) = g(\alpha t)$, *for any* $\epsilon_\eta, \epsilon_u, \epsilon_v > 0$, *there exists a time scaling factor* α *such that*

i) $\|\tilde{\eta}_u\|_{L_2} < \epsilon_\eta$

ii) $\|\bar{u}_d - u_d\|_{L_2} < \epsilon_u$

iii) $\|\bar{v}\|_{L_2} < \epsilon_v$.

Proof : To simplify the proof, the dimension of the unstable subsystem is assumed to be $n_u = 1$. In this case, both A_u and B_u become scalars. Let scalars a and b represent A_u and B_u, respectively. Substituting $\bar{v}$ into (2.49) yields

$$\dot{\tilde{\eta}}_u = -A_u\tilde{\eta}_u - 2\dot{\eta}_u. \tag{2.50}$$

From (2.39), for the noncausal signal $\eta_u(t)$, the bilateral Laplace transform is given by

$$\dot{\eta}_u(s) = \frac{bs}{s-a} y_d^{(r)}(s), \tag{2.51}$$

where the regions of convergence is $Re(s) < a$ with $a > 0$.

From (2.50), the Laplace transform of $\tilde{\eta}_u$ is given by

$$\tilde{\eta}_u(s) = \frac{-2}{s+a}\dot{\eta}_u(s) = \frac{-2bs}{s^2-a^2} y_d^{(r)}(s),$$

where the regions of convergence are $-a < Re(s) < a$ with $a > 0$.

Letting

$$H_1(s) = \frac{-2bs}{s^2-a^2}, \quad H_2(s) = \frac{bs}{s-a},$$

gives

$$\tilde{\eta}_u(s) = H_1(s) y_d^{(r)}(s), \quad \dot{\eta}_u(s) = H_2(s) y_d^{(r)}(s)$$

(i) Given a low pass signal $g(t)$, there exists a time scaling factor $\alpha_1 > 0$, such that $y_d^{(r)}(t)$ can be chosen as

$$y_d^{(r)}(t) = g(\alpha_1 t).$$

Then

$$g(\omega) = \mathcal{F}(g(t)), \quad H_1(\omega) = H_1(s)|_{s=j\omega}.$$

Furthermore, by the scaling property of the Fourier transform, it follows

$$y_d^{(r)}(\omega) = \mathcal{F}(g(\alpha_1 t)) = \frac{1}{\alpha_1} g(\frac{\omega}{\alpha_1}).$$

Since both $H_1(\omega)$ and $y_d^{(r)}(\omega)$ are bounded, set $K_1 = \|y_d^{(r)}(\omega)\|_\infty^2 + \|H_1(\omega)\|_\infty^2$, where K_1 is finite and $K_1 > 0$. Notice that

$$\int_{\omega_1}^{\infty} |g(\omega)|^2 d\omega \to 0, \quad \text{as} \quad \omega_1 \to \infty.$$

Thus, $\forall \epsilon_\eta > 0$, there exists $\omega_1(\epsilon_\eta)$ such that

$$\int_{\omega_1}^{\infty} |g(\omega)|^2 d\omega < \frac{\pi \epsilon_\eta^2}{K_1}.$$

Similarly, $\forall \epsilon_\eta > 0$, there exists $\omega_2(\epsilon_\eta)$ such that

$$\int_{0}^{\omega_2} |H_1(\omega)|^2 d\omega < \frac{\pi \epsilon_\eta^2}{K_1}.$$

Given ω_2, $\forall \epsilon_\eta > 0$, there exists α_1 such that $\alpha < \alpha_1$

$$\int_{\omega_2}^{\infty} |y_d^{(r)}(\omega)|^2 d\omega < \frac{\pi \epsilon_\eta^2}{K_1}.$$

The spectral separation is shown in Figure 2.2.

Consequently,

$$\begin{aligned}
\int_0^\infty |\tilde{\eta}(\omega)|^2 d\omega &= \int_0^{\omega_2} |H_1(\omega) y_d^{(r)}(\omega)|^2 d\omega + \int_{\omega_2}^\infty |H_1(\omega) y_d^{(r)}(\omega)|^2 d\omega \\
&\leq \|y_d^{(r)}(\omega)\|_\infty^2 \int_0^{\omega_2} |H_1(\omega)|^2 d\omega + \|H_1(\omega)\|_\infty^2 \int_{\omega_2}^\infty |y_d^{(r)}(\omega)|^2 d\omega \\
&< \frac{\pi \epsilon_\eta^2}{K_1} (\|y_d^{(r)}(\omega)\|_\infty^2 + \|H_1(\omega)\|_\infty^2) \\
&= \frac{\pi \epsilon_\eta^2}{K_1} K_1 = \pi \epsilon_\eta^2.
\end{aligned}$$

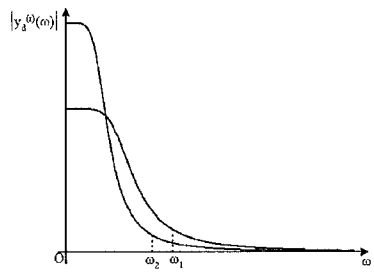

Figure 2.2 Spectral separation

Then by Parseval's theorem,

$$\begin{aligned} \|\tilde{\eta}_u(t)\|_{L_2}^2 &= \tfrac{1}{\pi}\int_0^\infty |\tilde{\eta}(\omega)|^2 d\omega \\ &< \tfrac{1}{\pi}\pi\epsilon_\eta^2 \\ &= \epsilon_\eta^2. \end{aligned}$$

It then follows

$$\|\tilde{\eta}_u(t)\|_{L_2} < \epsilon_\eta. \tag{2.52}$$

(ii) Furthermore, combining (2.36, 2.44) yields

$$\|\bar{u}_d - u_d\|_{L_2} = \|C_u\tilde{\eta}_u\|_{L_2}.$$

Note that C_u is a scalar in this case, and c can be used to represent C_u. Thus, it follows

$$\|\bar{u}_d - u_d\|_{L_2} < c\epsilon_\eta = \epsilon_u, \quad \text{where} \quad \epsilon_u > 0.$$

(iii) Similarly, given the low pass signal $g(t)$, there exists a time scaling factor $\alpha_2 > 0$ such that $y_d^{(r)}(t)$ can be chosen as

$$y_d^{(r)}(t) = g(\alpha_2 t).$$

Then

$$g(\omega) = \mathcal{F}(g(t)), \quad H_2(\omega) = H_2(s)|_{s=j\omega}$$

Furthermore,

$$y_d^{(r)}(\omega) = \mathcal{F}(g(\alpha_1 t)) = \tfrac{1}{\alpha_2} g(\tfrac{\omega}{\alpha_2}).$$

Since both $H_2(\omega)$ and $y_d^{(r)}(\omega)$ are bounded, set $K_2 = \|y_d^{(r)}(\omega)\|_\infty^2 + \|H_2(\omega)\|_\infty^2$, where K_2 is finite and $K_2 > 0$. Notice that

$$\int_{\omega_1'}^{\infty} |g(\omega)|^2 d\omega \to 0 \quad \text{as} \quad \omega_1' \to \infty.$$

Thus, $\forall \epsilon_1 > 0$, there exists $\omega_1'(\epsilon_1)$ such that

$$\int_{\omega_1'}^{\infty} |g(\omega)|^2 d\omega < \frac{\pi\epsilon_1^2}{K_2}$$

and $\forall \epsilon_1 > 0$, there exists $\omega_2'(\epsilon_1)$ such that

$$\int_0^{\omega_2'} |H_1(\omega)|^2 d\omega < \frac{\pi\epsilon_1^2}{K_2}.$$

Given ω_2', $\forall \epsilon_1 > 0$, there exists α_2 such that $\alpha < \alpha_2$

$$\int_{\omega_2'}^{\infty} |y_d^{(r)}(\omega)|^2 d\omega < \frac{\pi\epsilon_1^2}{K_2}.$$

By the same argument,

$$\begin{aligned} \int_0^{\infty} |\dot{\eta}(\omega)|^2 d\omega &= \int_0^{\omega_2} |H_2(\omega) y_d^{(r)}(\omega)|^2 d\omega + \int_{\omega_2}^{\infty} |H_2(\omega) y_d^{(r)}(\omega)|^2 d\omega \\ &\leq \|y_d^{(r)}(\omega)\|_\infty^2 \int_0^{\omega_2} |H_2(\omega)|^2 d\omega + \|H_2(\omega)\|_\infty^2 \int_{\omega_2}^{\infty} |y_d^{(r)}(\omega)|^2 d\omega \\ &= \pi\epsilon_1^2. \end{aligned}$$

Then, by Parseval's theorem, it immediately follows

$$\|\dot{\eta}_u(t)\|_{L_2} < \epsilon_1. \tag{2.53}$$

As a result, Equation (2.41) can be rewritten as follows

$$\begin{aligned} \bar{v} &= -2A_u\bar{\eta}_u - 2B_u y_d^{(r)} \\ &= -2A_u\bar{\eta}_u + 2A_u\eta_u - 2A_u\eta_u - 2B_u y_d^{(r)} \\ &= -2A_u(\bar{\eta}_u - \eta_u) - 2(A_u\eta_u + 2B_u y_d^{(r)}) \\ &= -2A_u\tilde{\eta}_u - 2\dot{\eta}_u, \end{aligned}$$

where in the last step, (2.39) is employed.

This then yields

$$\begin{aligned} \|\bar{v}\|_{L2} &\leq 2a\|\tilde{\eta}_u\|_{L_2} + 2\|\dot{\eta}_u\|_{L_2} \\ &< 2a\epsilon_\eta + 2\epsilon_1 \\ &= \epsilon_v, \quad \text{where} \quad \epsilon_v > 0. \end{aligned}$$

Choosing $\alpha = \min(\alpha_1, \alpha_2)$, then all the conclusions can be obtained.

Q.E.D.

Note that the proposed theorem easily extends to the $n_u > 1$ case.

Remark :

The same strategy can also be applied to the nonlinear case. By proper scaling, the rate of change of $y_d^{(r)}$ can be made arbitrarily small. In doing so, the equations (2.12, 2.13,2.14, 2.17) become quasi static. Let $\eta_{sq}, \eta_{uq}, \bar{\eta}_{sq}$, and $\bar{\eta}_{uq}$ denote the quasi static solutions of the dynamic (2.12, 2.13, 2.14, 2.17); that is, the solutions of (2.12, 2.13, 2.14, 2.15) can be written as

$$0 = A_s\eta_s + B_s y_d^{(r)} + d_s(y_d^{(r)}, \xi_d, \eta_s, \eta_u), \quad \eta_s(\pm\infty) = 0 \tag{2.54}$$

$$0 = A_u\eta_u + B_u y_d^{(r)} + d_u(y_d^{(r)}, \xi_d, \eta_s, \eta_u), \quad \eta_u(\pm\infty) = 0 \tag{2.55}$$

$$0 = A_s\bar{\eta}_s + B_s y_d^{(r)} + d_s(y_d^{(r)}, \bar{\xi}_d, \bar{\eta}_s, \bar{\eta}_u), \quad \bar{\eta}_s(0) = 0 \tag{2.56}$$

$$0 = A_u\bar{\eta}_u + B_u y_d^{(r)} + d_u(y_d^{(r)}, \bar{\xi}_d, \bar{\eta}_s, \bar{\eta}_u) + \bar{v}, \quad \bar{\eta}_u(0) = 0. \tag{2.57}$$

Then the true solutions of (2.12, 2.13, 2.14, 2.15) can be written as

$$\eta_s = \eta_{sq} + \epsilon_s \tag{2.58}$$

$$\eta_u = \eta_{uq} + \epsilon_u \tag{2.59}$$

$$\bar{\eta}_s = \bar{\eta}_{sq} + \bar{\epsilon}_s \tag{2.60}$$

$$\bar{\eta}_u = \bar{\eta}_{uq} + \bar{\epsilon}_u, \tag{2.61}$$

where $\epsilon_s, \epsilon_u, \bar{\epsilon}_s, \bar{\epsilon}_u > 0$, and can be made arbitrarily small by making $y_d^{(r)}$ arbitrarily slow.

By comparing (2.54) and (2.56), and (2.55) and (2.57) respectively, we notice that they are the same equations. In other words,

$$\eta_{sq} = \bar{\eta}_{sq} \tag{2.62}$$

$$\eta_{uq} = \bar{\eta}_{uq}. \tag{2.63}$$

Furthermore, it yields

$$\|\bar{\eta}_s - \eta_s\|_{L_2} = \|\tilde{\eta}_s\|_{L_2} < \epsilon_{ns} \tag{2.64}$$

$$\|\bar{\eta}_u - \eta_u\|_{L_2} = \|\tilde{\eta}_u\|_{L_2} < \epsilon_{nu}. \tag{2.65}$$

Therefore, by processing scaling, the difference of $\bar{\eta}_u$ and η_u is arbitrarily small; that is, $\bar{\eta}_u \to \eta_u$ as $t \to \infty$.

Suppose the causal inversion of nonlinear systems can be solved, since $\|\tilde{\eta}_s\|_{L_2} < \epsilon_{ns}$ and $\|\tilde{\eta}_u\|_{L_2} < \epsilon_{nu}$, and the system has a well-defined relative degree at the equilibrium point zero, then $\psi(x) = [\xi^T \quad \eta^T]^T = [\xi^T, \quad [\eta_s \quad \eta_u]P_1^T]^T$ defines a local diffeomorphism. Its inverse is $x = \phi(\xi, \eta)$. $\bar{\eta}$ has been defined as $\bar{\eta} = P_1[\bar{\eta}_s \quad \bar{\eta}_u]^T$, thus given an $\epsilon_u > 0$, $\bar{u}_d$ can be found such that

$$\|\bar{u}_d - u_d\|_{L_2} < \epsilon_u.$$

Furthermore, given an $\epsilon_v > 0$, the following inequality is also satisfied

$$\|\bar{v}\|_{L_2} < \epsilon_v.$$

Therefore, the conditions for the linear case also apply to the nonlinear case.

2.4 Output Tracking Control

When defining $\tilde{x}(t) = \bar{x}_d(t) - x(t)$, $\tilde{u}(t) = \bar{u}_d(t) - u(t)$, and $\tilde{y} = y_d(t) - y(t)$, the error dynamics for (2.1) are given as follows:

$$\begin{aligned} \dot{\tilde{x}} &= f(\tilde{x}) + g(\tilde{x})u + g(\bar{x}_d)\tilde{u} + P_{\bar{v}}\bar{v} \\ \tilde{y} &= h(\tilde{x}), \end{aligned} \tag{2.66}$$

where $f(\tilde{x}) = f(\bar{x}_d) - f(x), g(\tilde{x}) = g(\bar{x}_d) - g(x)$, and $h(\tilde{x}) = h(\bar{x}_d) - h(x)$.
Since the design goal is to achieve *stable* $\epsilon-$*tracking* so that

$$\|\tilde{y}\|_{L_2} < \epsilon \quad \text{as} \quad t \to \infty,$$

with bounded $x(t)$, an H_∞ controller is the natural choice. Suppose the closed-loop nonlinear mapping from $\bar{v}$ to $\tilde{y}$ is given by

$$\tilde{y} = \Phi(\cdot)\bar{v}. \tag{2.67}$$

If an H_∞ controller $K(\cdot)$ could be found, it would give

$$\|\tilde{y}\|_{L_2} \leq \|\Phi(\cdot)\|_\infty \|\bar{v}\|_{L2}.$$

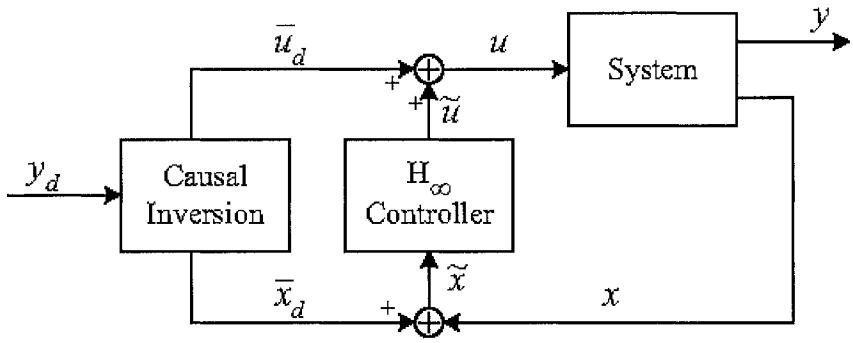

Figure 2.3 Block diagram of close-loop system

Since $\|\Phi(\cdot)\|_\infty \|\bar{v}\|_{L2}$ is bounded, this implies $\|\tilde{y}\|_{L_2} < \gamma\epsilon_v = \epsilon$ with $\epsilon > 0$ as $t \to \infty$. From the definition of causal inversion, $\bar{x}_d$ is bounded, then $\tilde{x}$ is also bounded by Assumption A1 if H_∞ controller is appropriately designed. As a result, $x(t)$ must be bounded; therefore *stable* $\epsilon-$*tracking* is achieved. The block diagram of the closed-loop system is shown in Figure 2.3.

Similarly, the error dynamics for linear systems (2.28) are addressed as follows:

$$\begin{cases} \dot{\tilde{x}} = A\tilde{x} + B\tilde{u} + P_{\bar{v}}\bar{v} \\ \tilde{y} = C\tilde{x}. \end{cases} \tag{2.68}$$

Theorem 2 in Section 2.3.2 has provided the causal inversion solution for linear systems. And given an $\epsilon_v > 0$, $\|\bar{v}\|_{L2} < \epsilon_v$ with $\epsilon_v > 0$ can be made.

An H_∞ controller is required to design for these linear systems. Suppose the closed-loop transfer function from $\bar{v}$ to $\tilde{y}$ is given by the linear fractional transformation

$$\tilde{y} = F_l(G, K)\bar{v}. \tag{2.69}$$

Let $K(s)$ be the H_∞ controller that minimizes the gain from $\bar{v}$ and $\tilde{y}$ (see Figure 2.3), where $\tilde{G}$ is the general plant and K is the controller. This would then yield

$$\|\tilde{y}\|_{L_2} \leq \|F_l(G, K)\|_\infty \|\bar{v}\|_{L2} < \gamma\epsilon_v = \epsilon, \quad \text{where} \quad \epsilon > 0.$$

This implies stable ϵ-tracking is achieved, which indicates that the total energy in the transient tracking error can be controlled within any given requirement.

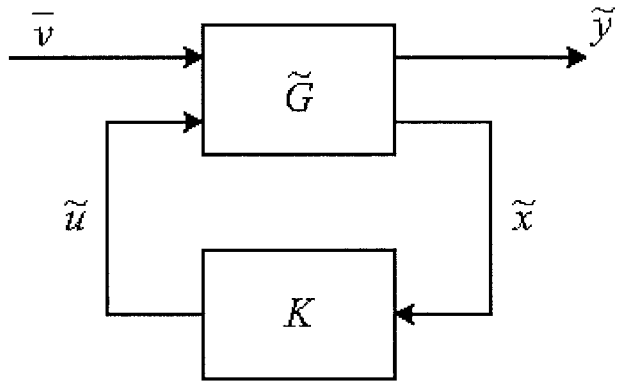

Figure 2.4 Control configuration for linear systems

2.5 An Example: A One-Link Flexible Manipulator

A closed-loop controller for a one-link flexible manipulator is designed in this section using causal inversion.

2.5.1 Dynamics Model

A nonlinear one-link flexible manipulator model is obtained from [10]. A simple modelling technique divides the flexible link into rigid segments that are connected by elastic springs, where link deformation is concentrated. The following treatment will be limited to the case of two equal segments of uniform mass moving along the horizontal plane.

Let m and l denote the total link mass and length, k the spring elasticity, and u the input torque. With reference to Figure 2.5,oq_1q_2 is a fixed reference frame, θ_1 is the angular position of the link base, while θ_2 is the flexible variable. The dynamic equations are

$$\begin{bmatrix} b_{11}(\theta_2) & b_{12}(\theta_2) \\ b_{12}(\theta_2) & b_{22} \end{bmatrix} \begin{bmatrix} \ddot{\theta}_1 \\ \ddot{\theta}_2 \end{bmatrix} + \begin{bmatrix} c_1(\theta_2, \dot{\theta}_1, \dot{\theta}_1) \\ c_2(\theta_1, \dot{\theta}_1) + k\theta_2 + d_2\dot{\theta}_2 \end{bmatrix} = \begin{bmatrix} 1 \\ 0 \end{bmatrix} u \qquad (2.70)$$

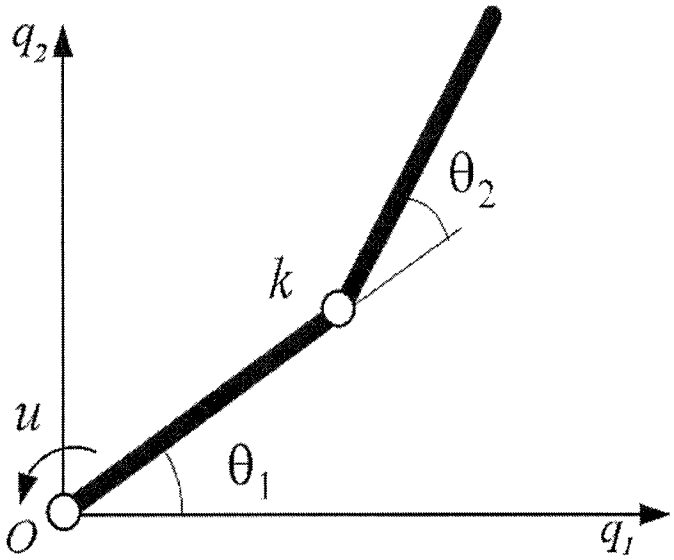

Figure 2.5 A simple one-link flexible manipulator

with the elements of the inertia matrix $B(\theta_2)$ given by

$$b_{11}(\theta_2) = a + 2c\cos(\theta_2)$$
$$b_{12}(\theta_2) = b + c\cos(\theta_2)$$
$$b_{22} = b$$

and Coriolis and centrifugal terms

$$c_1(\theta_2, \dot{\theta}_1, \dot{\theta}_2) = -c(\dot{\theta}_2^2 + 2\dot{\theta}_1\dot{\theta}_2)\sin(\theta_2)$$
$$c_2(\theta_2, \dot{\theta}_1) = c\dot{\theta}_1^2\sin(\theta_2),$$

where

$$a = 5m\ell^2/24, \;\; b = m\ell^2/24, \;\; c = m\ell^2/16.$$

In (2.70), d_1 and d_2 are damping coefficients representing viscous friction at the joint and link structural (passive) dissipation, respectively. State equations can be obtained by setting $x = (\theta_1, \theta_2, \dot{\theta}_1, \dot{\theta}_2)^T \in \Re^4$.

The linearized expression of the end-effector angular position, as seen from the base,

$$y = \theta_1 + \frac{1}{2}\theta_2 \tag{2.71}$$

will be taken as the controlled output for the system.

Linearizing the above dynamics model for this one-link flexible manipulator yields

$$\begin{bmatrix} \dot{\theta}_1 \\ \dot{\theta}_2 \\ \ddot{\theta}_1 \\ \ddot{\theta}_2 \end{bmatrix} = \begin{bmatrix} 0 & 0 & 1 & 0 \\ 0 & 0 & 0 & 1 \\ 0 & \frac{(b+c)k}{ab-b^2-c^2} & \frac{-bd_1}{ab-b^2-c^2} & \frac{(b+c)d_2}{ab-b^2-c^2} \\ 0 & \frac{-(a+2c)k}{ab-b^2-c^2} & \frac{(b+c)d_1}{ab-b^2-c^2} & \frac{-(a+2c)d_2}{ab-b^2-c^2} \end{bmatrix} \begin{bmatrix} \theta_1 \\ \theta_2 \\ \dot{\theta}_1 \\ \dot{\theta}_2 \end{bmatrix} + \begin{bmatrix} 0 \\ 0 \\ \frac{b}{ab-b^2-c^2} \\ \frac{-b-c}{ab-b^2-c^2} \end{bmatrix} u \tag{2.72}$$

$$y = [1 \quad \frac{1}{2} \quad 0 \quad 0][\theta_1, \theta_2, \dot{\theta}_1, \dot{\theta}_2]^T.$$

In the following section, a casual inversion-based controller will be designed for this linearized model.

2.5.2 Controller Design

In the system after inversion, the input-output linearizing coordinates are $\tilde{x} = (y, \dot{y}, \theta_2, \dot{\theta}_2)$. A linear transformation in state space $\Psi(x)$ can be expressed as follows:

$$\Psi(x) \triangleq \begin{bmatrix} y \\ \dot{y} \\ \theta_2 \\ \dot{\theta}_2 \end{bmatrix} = \begin{bmatrix} 1 & \frac{1}{2} & 0 & 0 \\ 0 & 0 & 1 & \frac{1}{2} \\ 0 & 1 & 0 & 0 \\ 0 & 0 & 0 & 1 \end{bmatrix} \begin{bmatrix} \theta_1 \\ \theta_2 \\ \dot{\theta}_1 \\ \dot{\theta}_2. \end{bmatrix}. \tag{2.73}$$

Then the zero dynamics driven by the reference output trajectory can be obtained and written in the following state-space form by setting $y(t) \equiv y_d(t)$,

$$\begin{bmatrix} \dot{\theta}_2 \\ \ddot{\theta}_2 \end{bmatrix} = A_\eta \begin{bmatrix} \dot{\theta}_2 \\ \ddot{\theta}_2 \end{bmatrix} + B_\eta \ddot{y}_d, \tag{2.74}$$

where

$$A_\eta = \begin{bmatrix} 0 & 1 \\ \frac{2k}{c-b} & \frac{2d_2}{c-b} \end{bmatrix}, \quad B_\eta = \begin{bmatrix} 0 \\ \frac{2(b+c)}{c-b} \end{bmatrix}.$$

Moreover, $k > 0$, and $d_2 > 0$. Since $c > b$, and $c - b > 0$, it is seen that the zero dynamics is unstable, which means the system is a nonminimum phase system.

There exists a linear transformation

$$\begin{bmatrix} \theta_2 \\ \dot{\theta}_2 \end{bmatrix} = P_1 \begin{bmatrix} \eta_s \\ \eta_u \end{bmatrix}, \tag{2.75}$$

which transforms (2.74) into

$$\begin{cases} \dot{\eta}_s = A_s\eta_s + B_s\ddot{y}_d \\ \dot{\eta}_u = A_u\eta_u + B_u\ddot{y}_d. \end{cases} \tag{2.76}$$

Two dynamic equations are defined as follows:

$$\begin{cases} \dot{\bar{\eta}}_s = A_s\bar{\eta}_s + B_s\ddot{y}_d, \;\; \bar{\eta}_s(0) = 0 \\ \dot{\bar{\eta}}_u = A_u\bar{\eta}_u + B_u\ddot{y}_d + \bar{v}, \;\; \bar{\eta}_u(0) = 0. \end{cases} \tag{2.77}$$

By choosing $\bar{v} = -2A_u\bar{\eta}_u - 2B_u\ddot{y}_d$ and solving the following equations:

$$\begin{cases} \dot{\bar{\eta}}_s = A_s\bar{\eta}_s + B_s\ddot{y}_d, \;\; \bar{\eta}_s(0) = 0 \\ \dot{\bar{\eta}}_u = -A_u\bar{\eta}_u - B_u\ddot{y}_d, \;\; \bar{\eta}_u(0) = 0, \end{cases} \tag{2.78}$$

the bounded $\bar{\eta}_s$ and $\bar{\eta}_u$ can be obtained. Moreover, since $[\theta_{2d} \;\; \dot{\theta}_{2d}]^T = P_1[\bar{\eta}_s \;\; \bar{\eta}_u]^T$, it follows that

$$\begin{bmatrix} \theta_{1d} \\ \theta_{2d} \\ \dot{\theta}_{1d} \\ \dot{\theta}_{2d} \end{bmatrix} = \begin{bmatrix} 1 & 0 & -0.5 & 0 \\ 0 & 0 & 1 & 0 \\ 0 & 1 & 0 & -0.5 \\ 0 & 0 & 0 & 1 \end{bmatrix} \begin{bmatrix} y_d \\ \dot{y}_d \\ \theta_{2d} \\ \dot{\theta}_{2d} \end{bmatrix}. \tag{2.79}$$

The nominal input is then calculated by

$$\bar{u}_d = d_1\dot{\theta}_{1d} + \tfrac{a-2b}{b}(k\theta_{2d} + d_2\dot{\theta}_{2d}) + \tfrac{2(ab-b^2)}{b}\ddot{y}_d.$$

The controller is composed by the following structure

$$u = \bar{u}_d + K(\bar{x}_d - x), \tag{2.80}$$

where $\bar{x}_d$ denotes the state variables of the forward dynamics, $\bar{x}_d = (\theta_{1d}, \theta_{2d}, \dot{\theta}_{1d}, \dot{\theta}_{2d})$. Then a standard H_∞ optimal controller is designed to find the stabilizing controller K for stabilizing the forward dynamics.

2.5.3 Simulation Results

The parameters for the one-link flexible manipulator were chosen the same as in De Luca [10]. $l = 1$ m, $m = 0.2$ kg, $k = 5$ N $\cdot$ m/rad, and $d_1 = d_2 = 0.01$ N $\cdot$ m $\cdot$ sec/rad.

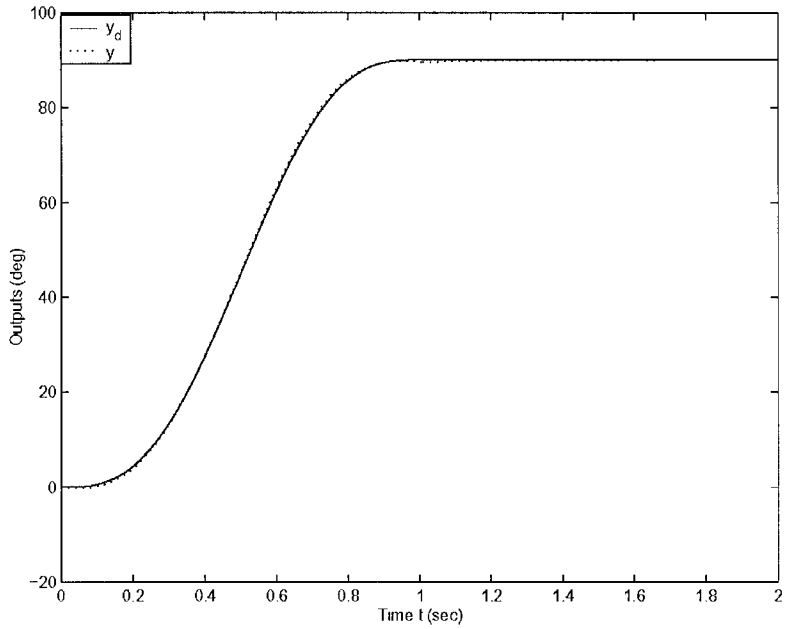

Figure 2.6 Desired (solid) and actual (dotted) output trajectories for Case 1

Let the desired output trajectory be defined as follows:

$$y_d = \begin{cases} \frac{\pi}{2t_f}t - \frac{1}{4}\sin(\frac{2\pi}{t_f}t), & 0 \leq t \leq t_f \\ \frac{\pi}{2}, & t > t_f \end{cases}$$

as shown by the solid curve in Figure 2.6.

For the given trajectory, the following data were used: $y_0 = 0^o, y_f = 90^o$. The initial conditions are $\theta_1 = \theta_2 = \dot{\theta}_1 = \dot{\theta}_2 = 0$. Two cases are simulated below.

Case 1 : $t_f = 1$ second and **Case 2** : $t_f = 0.5$ seconds.

The desired and actual trajectories of the output for Cases 1 and 2 are shown in Figures 2.6 and 2.7 respectively. The output tracking errors for Cases 1 and 2 are shown in Figures 2.8 and 2.9 respectively. The maximum error during transients for Case 1 is relatively small (around 0.7^o); whereas, the maximum error during transients for Case 2 is around 3.5^o, which is significantly larger than in Case 1.

Furthermore, when applied to a one-link flexible manipulator, causal inversion has the advantages of not requiring the preloading for the links (as does stable inversion), as well as eliminating the need to solve a set of nontrivial partial differential algebraic

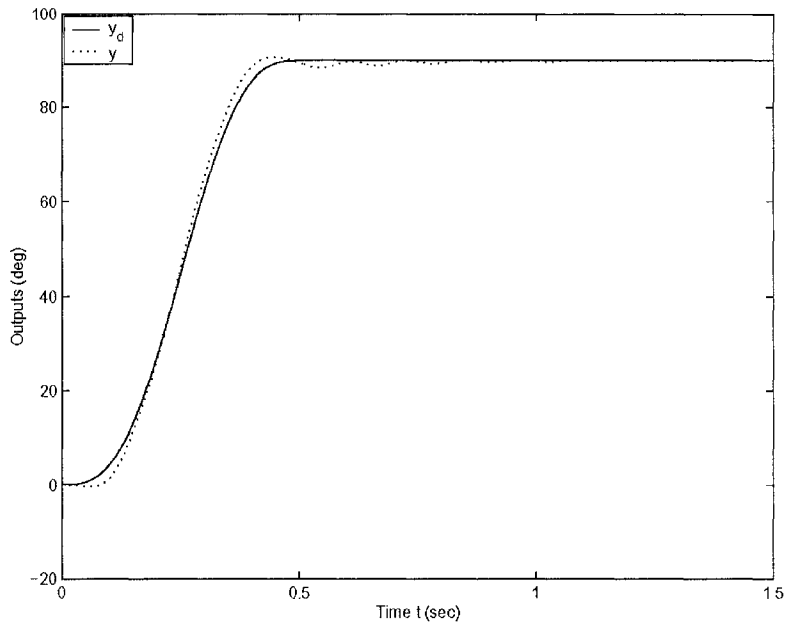

Figure 2.7 Desired (solid) and actual (dotted) output trajectories for Case 2

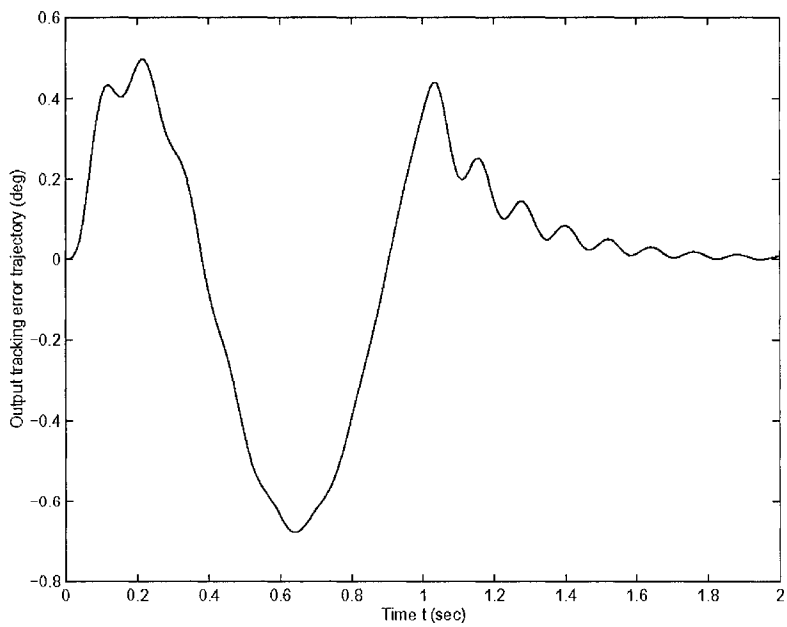

Figure 2.8 Output tracking error trajectory for Case 1

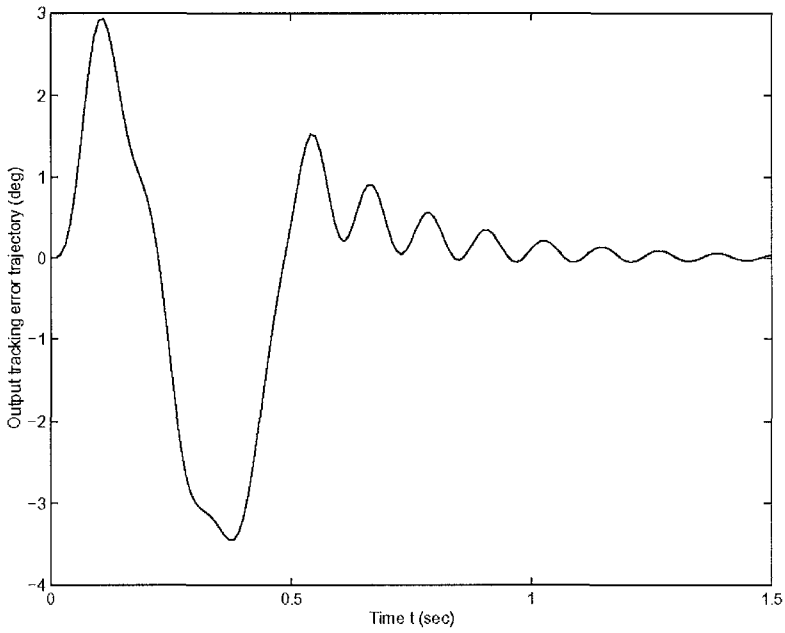

Figure 2.9 Output tracking error trajectory for Case 2

equations (as required by the nonlinear regulation approach).

2.6 Conclusions

This paper introduces a new procedure for designing a nonminimum phase output tracking controller driven by a causal reference profile. The output tracking controller has a feed-forward structure with feedback. In this approach, the nonminimum phase system is first stably inverted on-line to obtain both desired state and input trajectories that map exactly into the desired output trajectory. Then an H_∞ optimal controller is used to stabilize the closed-loop system. This new controller achieves stable ϵ—-tracking. This new approach provides causal solutions and avoids solving the nontrivial PDEs. As an example, a causal inversion-based controller is designed for tip trajectory tracking of a one-link flexible manipulator. Simulation results demonstrate that the causal inversion approach is very effective for obtaining output tracking for flexible manipulators. This new approach has many important engineering applications such as in rocket tracking and aircraft altitude control problems. Future work will continue to

explore new applications of causal inversion.

Bibliography

[1] R. Brockett and M. Mesarovic, "The reproducibility of multivariable systems," *J. Math. Anal. Appl.*, vol. 11, pp. 548-563, 1965.

[2] D. Chen and B. Paden, "Stable inversion of nonlinear non-minimum phase systems," *Proc. of Japan/USA Symposium on Flexible Automation*, pp. 791-797, 1992.

[3] D. Chen, "An iterative solution to stable inversion of nonlinear non-minimum phase systems," *American Control Conference*, pp. 2960-2964, 1993.

[4] D. Chen, "Output tracking control of nonlinear nonminimum phase systems," *Conference on Decision and Control*, pp. 2340-2345, 1994.

[5] S. Devasia, D. Chen, and B. Paden, "Nonlinear inversion-based output tracking," *IEEE Trans. Automat. Contr.*, vol. 41, pp. 930-942, 1996.

[6] R. Hirschorn, "Invertibility of nonlinear control systems," *SIAM J. Contr. Optim.*, vol. 17, no. 2, pp. 289-297, 1979.

[7] A. Isidori, *Nonlinear Control Systems: An Introduction*, Springer-Verlag, New Jersey, 1989.

[8] A. Isidori and C. Byrnes, "Output regulation of nonlinear systems," *IEEE Trans. Automat. Contr.*, vol. 35, pp. 131-140, 1990.

[9] H. Khalil, *Nonlinear Systems*, Prentice Hall, Upper Saddle River, New Jersey, 1996.

[10] A. De Luca, L. Lanari, and G. Ulivi, "Nonlinear regulation of end-effector motion for a flexible robot arm," *New Trends in Systems Theory*, Genova, Italy, July 9-11, 1990.

[11] L. Silverman, "Inversion of multivariable linear systems," *IEEE Trans. Automat. Contr.*, vol. 14, pp. 270-276, 1969.

[12] S. Singh, "A modified algorithm for invertibility in nonlinear systems," *IEEE Trans. Automat. Contr.*, vol. AC-26, pp. 595-599, 1981.

[13] W. Wonham, *Linear Multivariable Control: A Geometric Approach*, Springer-Verlag, New York, 1985.

[14] X. Wang and D. Chen, "Causal inversion for non-minimum phase systems," 40^{th} *IEEE Conference on Decision and Control*, pp. 73-78, 2001.

3 Adaptive Learning Control for Nonminimum Phase Systems

Abstract — In this paper, a new adaptive learning algorithm is presented for the repetitive tracking control of a class of unstable nonminimum phase systems. After each repetitive trial, a Least-Squares method is used to estimate the system parameters. The output tracking error and the identified system model are used through stable inversion to find the feed forward input, together with the desired state trajectories, for the next trial. An adaptive backstepping based tracking controller is used in each trial to ensure the regulation of the desired state trajectories. Simulation results demonstrate that the proposed learning control scheme is very effective in reproducing the desired trajectories.

3.1 Introduction

Iterative learning control (ILC) is a feed forward control approach aimed at achieving high performance output tracking control by "learning" from past experience so as to eliminate the repetitive errors from future execution [9]. This approach was motivated by the observation that human beings are able to improve performance through repeated practice. Since a learning controller is able to eliminate the repetitive errors that exist when using a servo controller alone, it has great potential in future robotic systems.

The concept of iterative learning control was first introduced by Arimoto et al. [1]. It is based on the use of repeated trials to track a desired trajectory. At each trial, the system input and output signals are stored. The learning control algorithm then evaluates the performance error. Based on the error signal, the learning controller computes a new input signal, which is stored for use during the next trial. The new input is chosen such that the performance error will be reduced in the next trial. One of the important

features of iterative learning control is that it requires little *a priori* knowledge about the controlled system during the controller design phase.

Arimoto's original learning controller is called a D-type algorithm. Since then, many researchers have proposed various learning control schemes. Moore extended Arimoto's method to systems with a relative degree higher than one [9]. Hauser presented a nonlinear version of Arimoto's method for a class of nonlinear systems [5]. Application of this type of learning controller to robotics was reported in many studies such as [2] and [7]. The basic and succinct exposition of ILC is surveyed in [10].

Although existing learning algorithms have been theoretically proven to provide output error convergence and have had successful applications, many such algorithms have practical difficulties with nonminimum phase systems [3]. An adaptive learning algorithm that works for nonminimum phase systems was recently developed by Gao and Chen [3]. In this paper, an adaptive learning algorithm is further developed to work for unstable nonminimum phase systems. Simulation results are presented to show the effectiveness of the proposed adaptive learning algorithm.

The remainder of the paper is organized as follows. In the next section we define a class of desired trajectories under consideration and state the problem of ILC. Section 3 presents the new adaptive learning control law. Section 4 contains simulation results. Finally, some conclusion remarks are given in Section 5.

3.2 Problem Statement

Consider a system dynamics in the k^{th} trial:

$$\dot{x}_k = f(x_k, \theta, u_k) \tag{3.1}$$

$$y_k = h(x_k, \theta, u_k) \tag{3.2}$$

where x_k is defined on a neighborhood X of the origin of $\Re^n$, θ is a parameter vector, with input $u_k \in \Re^m$ and output $y_k \in \Re^p$. The mappings f and g are smooth in x_k and u_k, with $f(0, \theta, 0) \equiv 0$ and $h(0, \theta, 0) \equiv 0$.

We make the following assumptions:

(A1) The system has a well-defined relative degree $r = (r_1, \cdots, r_m)^T$ which is known. The linearization of the system about an equilibrium point, which is assumed to be the origin WLOG, is completely controllable.

(A2) The order of the system, n, is known.

(A3) The system parameter vector θ is unknown or known incompletely.

(A4) A desired output trajectory is given and is a sufficiently smooth function of t satisfying $y_d(t) = 0$ for any $t \in (-\infty, 0] \cup [T, \infty)$ and finite for any $t \in (0, T)$, where $T > 0$.

Note: In (A4), sufficiently smooth means that the signal has continuous derivatives of any order up to the relative degree. (A4) also requires $y_d(t)$ having a compact support $[0, T]$.

Iterative Learning Control Problems :

Given a desired output trajectory $y_d(t)$ and a tolerance error bound ϵ for a class of system (1) and (2), starting from an arbitrary continuous initial control input $u_0^d(\cdot)$ and initial state $x_0^d(\cdot)$, iterative learning control is to find a sequence of desired state trajectory $x_k^d(\cdot)$ and desired control inputs $u_k^d(\cdot)$, which when applied to the system, produces an output sequence $y_k(\cdot)$ such that

(1) $\|y_d(\cdot) - y_k(\cdot)\|_\infty \leq \epsilon$, as $k \to \infty$, where k is the trial number and $\|f\|_\infty = \sup_{t\in[0,T]} \|f(t)\|$.

(2) $\|u_k^d(t)\| \leq \epsilon, \|x_k^d(t)\| \leq \epsilon, \forall t \in (-\infty, 0] \cup [T, +\infty)$.

(3) $u_k^d(t)$, $x_k^d(t)$, $u_k(t)$, and $x_k(t)$ are uniformly bounded.

The system can be represented in terms of desired control input $u_k^d(\cdot)$ and output $y_k(\cdot)$ in the k^{th} trial by means of a nonlinear time-varying operator Π as follows:

$$y_k(\cdot) = \Pi(\cdot) u_k^d(\cdot) \tag{3.3}$$

In this dynamic process, the functions have two arguments: continuous time t and the trial number k. In the sequel it is assumed that the variation of the operator over two consecutive trials is slow and can be neglected. Then the operator obtained by identification performed in the k^{th} trial can be used to determine the input for the $(k+1)^{th}$ trial. This general description of the problem allows a simultaneous description

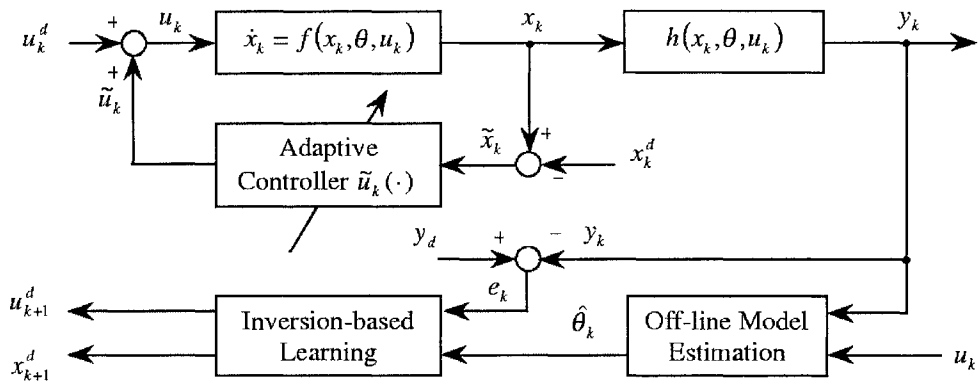

Figure 3.1 Block diagram of adaptive learning control system

of linear or nonlinear dynamics, continuous or discrete plant, and time-invariant or time-varying systems.

For applying linear ILC, however, the plant must fulfill the following conditions: (1) The desired trajectory $y_d(t)$ is identical for every trial and satisfies Assumption (A4). (2) Each trial has the fixed period T. (3) The system parameters are fixed or very slowly time-varying.

3.3 Adaptive Learning Control

In section 2, we have given the general setup of learning control. In this section, an adaptive learning controller will be presented. The block diagram of the adaptive learning system is shown in Figure 3.1.

The proposed adaptive learning control strategy has three components: a parameter estimator, a stable inverse system, and an adaptive backstepping feedback controller. The parameter estimator is in charge of "learning" the parameterized model of the system. During each trial, the input and output trajectories are recorded. Then an off-line Least-Squares method is applied to obtain the optimal estimate of parameters. Also obtained during each trial is the output tracking error signal. This error signal and the estimated model are used by the stable inverse system to learn the optimal input signal for the next trial. Although the estimated model may be nonminimum phase which

normally leads to unbounded inverse solutions, stable inversion guarantees a unique and bounded inverse solution. This "learning" action is done "off-line" between two consecutive trials. Afterwards, the new feed forward input is used by the adaptive backstepping feedback controller to stabilize the system and to ensure regulation of the tracking error. The controller is designed following a recursive backstepping procedure and it takes advantage of the parametric strict-feedback structure of the system. The controller parameters are also continuously updated in real-time using an adaptive control law. The same feedback control algorithm is used during every trial. In the following, we give the implementation of the adaptive learning algorithm for continuous-time systems.

3.3.1 Solution to Stable Inversion of nonminimum Phase Systems

Consider a LTI system in the form:

$$\sum_1 : \begin{cases} \dot{x} = Ax + Bu \\ y = Cx + Du \end{cases}$$

Suppose an estimated model $\hat{G}$ is obtained. If it is minimum phase, one can obtain the desired feed forward input by

$$u^d = \hat{G}^{-1} y_d \tag{3.4}$$

However, if $\hat{G}$ is nonminimum phase, this will lead to unbounded solutions. The stable inversion theory [4] provides an avenue to overcome this difficulty. It was shown that under certain conditions, there exists a unique stable inverse system $\hat{H}$ of $\hat{G}$ such that the inverse solution $\hat{H}y_d$ is bounded and it reproduces y_d exactly when applied as an input to $\hat{G}$, that is,

$$\hat{G}(\hat{H}y_d) = y_d \tag{3.5}$$

Here, the procedure to obtain this unique stable inverse solution $u^d = \hat{H}y_d$ is illustrated. There are four steps:

(1) Find the time-domain state space model of $\hat{G}$:

Since $\hat{G}u^d = \hat{G}\hat{H}y_d = y_d$, a state-space representation of $\hat{G}$ yields

$$\dot{x}^d(t) = \hat{A}x^d(t) + \hat{B}u^d(t) \tag{3.6}$$

$$y_d(t) = \hat{C}x^d(t) + \hat{D}u^d(t) \tag{3.7}$$

where x^d is the state and $\hat{A}, \hat{B}, \hat{C}$, and $\hat{D}$ are matrices with suitable sizes.

(2) Find its inverse in state space:

Differentiate $y_d(t)$ until u^d appears explicitly in the right hand side. Solve for u^d and substitute it into (3.6) and (3.7) to obtain

$$\dot{x}^d(t) = \bar{A}x^d(t) + \bar{B}y_d^{(r)}(t) \tag{3.8}$$

$$u^d(t) = \bar{C}x^d(t) + \bar{D}y_d^{(r)}(t) \tag{3.9}$$

where $\bar{A}, \bar{B}, \bar{C}$, and $\bar{D}$ are defined according to the substitution.

(3) Decompose the inverse system into center, stable, and unstable subsystems:

Perform a change of variables so that

$$x^d = Pz = P[z^c, z^s, z^u]^T \tag{3.10}$$

which leads to

$$\dot{z}^c = A^c z^c + B^c y_d^{(r)} \tag{3.11}$$

$$\dot{z}^s = A^s z^s + B^s y_d^{(r)} \tag{3.12}$$

$$\dot{z}^u = A^u z^u + B^u y_d^{(r)} \tag{3.13}$$

$$u^d = [C^c \;\; C^s \;\; C^u][z^c \;\; z^s \;\; z^u]^T + \bar{D}y_d^{(r)} \tag{3.14}$$

where A^c, A^s, and A^u are real Jordan matrices of suitable dimensions; A^c has r eigenvalues at zero; A^s has all eigenvalues in the open left-half plane; A^u has all eigenvalues in the open right-half plane.

(4) Obtain the stable inverse system:

Pick the transformation matrix P so that the center subsystem is a simple chain of r integrators. Solve that and impose two boundary conditions on the stable and unstable

subsystems to yield

$$z^c = [y_d, \dot{y}_d, \cdots, y_d^{(r-1)}]^T \tag{3.15}$$

$$\dot{z}^s = A^s z^s + B^s y_d^{(r)}, t \geq 0; z^s(t) = 0, \quad \forall\, t \leq 0 \tag{3.16}$$

$$\dot{z}^u = A^u z^u + B^u y_d^{(r)}, t \leq T; z^u(t) = 0, \quad \forall\, t \geq T \tag{3.17}$$

These together with (3.10) and (3.14) define the desired stable inverse system.

In classical inversion, (3.8) and (3.9) are treated as a dynamic system. Since it is unstable for a nonminimum phase system, it leads to unbounded solutions for u^d. In contrast, the stable inverse system always yields bounded solutions for bounded and smooth y_d. This can be clearly seen from (3.15)-(3.17) since the center solution z^c is clearly bounded, the stable subsystem is in the forward time, and the unstable subsystem is in the reverse time, all leading to bounded solutions.

When the system is minimum phase, there will be no unstable subsystem. And the dimension of z^u and those of the associated matrices will be zero. Therefore, the proposed approach also applies to minimum phase systems.

In this paper, we only consider LTI systems in this form:

$$\sum\nolimits_2 : \begin{cases} \dot{x}_{i-1,k} = x_{i,k}; \;\; i = 2, 3, \cdots, n \\ \dot{x}_{n,k} = x_k^T a + u_k \\ y_k = C x_k \end{cases}$$

Based on the stable solutions outline presented above, to facilitate iterative learning, we modify the inversion process slightly as follows. Referring to Figure 1, let G denote the system operator from u_k to y_k. Let u_{k+1} be the new input for the next trial. Then the new tracking error signal will be

$$\begin{aligned} e_{k+1} &= y_d - G u_{k+1} \\ &= y_d - G(u_{k+1}^d + \tilde{u}_{k+1}) \\ &= e_k - G(u_{k+1}^d - u_k^d) - G(\tilde{u}_{k+1} - \tilde{u}_k) \end{aligned}$$

Then we get

$$e_{k+1} + G(\tilde{u}_{k+1} - \tilde{u}_k) = e_k - G u_{k+1}^e$$

where $u^e_{k+1} = u^d_{k+1} - u^d_k$.

The goal of designing a learning control law is to make $e_{k+1}(\cdot)$ gradually decrease as k increases. For any remaining errors, the feedback control action will try to reduce them. Therefore, we simply set $e_{k+1} = 0$ and $\tilde{u}_{k+1} - \tilde{u}_k = 0$ to design u^e_{k+1}. That is, we want

$$e_k = G u^e_{k+1} \tag{3.18}$$

Since G is unknown and $\hat{G}_k$ is the best estimate model after the k^{th} trial, we will use

$$u^e_{k+1} = \hat{H}_k e_k \tag{3.19}$$

$$x^e_{k+1} = P_k z = P_k [z^c, z^s, z^u]^T \tag{3.20}$$

so that $e_k = \hat{G}_k u^e_{k+1}$. Then our learning algorithm would be

$$u^d_{k+1} = u^d_k + u^e_{k+1} \tag{3.21}$$

$$x^d_{k+1} = x^d_k + x^e_{k+1} \tag{3.22}$$

As a further modification, one may introduce a forgetting factor α $(0 < \alpha < 1)$ and use:

$$u^d_{k+1} = u^d_k + \alpha u^e_{k+1} \tag{3.23}$$

$$x^d_{k+1} = x^d_k + \alpha x^e_{k+1} \tag{3.24}$$

where u^e_{k+1} and x^e_{k+1} are given by (3.19) and (3.20), which are the stable inverse solutions from e_k and $\hat{G}_k$. (Note that: in the rest of the paper, u^d, x^d, and u^e represent u^d_{k+1}, x^d_{k+1}, and u^e_{k+1} respectively for notational convenience).

However, the controller design in the next subsection will still assume $\alpha = 1$ so that u^d, x^d, and y_d satisfy the dynamics of $\hat{G}_k$, that is :

$$\sum\nolimits_3 : \begin{cases} \dot{x}^d_{i-1} = x^d_i; \;\; i = 2, \cdots, n \\ \dot{x}^d_n = \hat{a}^T_k x^d + u^d \\ y_d = \hat{C}_k x^d \end{cases}$$

3.3.2 Adaptive Backstepping Controller Design

There are a lot of methods to design a controller. Since the parameters of the systems are unknown, we need to design an adaptive controller. Here we follow a popular approach of adaptive backstepping design [8].

Define $\tilde{x}_k = x_k - x^d$ and $\tilde{u}_k = u_k - u^d$. For clarity, we will drop the subscript k in sections 3.2 and 3.3 if it does not cause confusion. One can easily verify:

$$\sum_4 : \begin{cases} \dot{\tilde{x}}_{i-1} = \tilde{x}_i; \;\; i = 2, \cdots, n \\ \dot{\tilde{x}}_n = \tilde{x}^T a + [a - \hat{a}]^T x^d + \tilde{u} \end{cases}$$

The goal is to design $\tilde{u}$ to guarantee the regulation of $\tilde{x}$. Since a is unknown, let $\vartheta(t)$ be the on-line estimate of a and rewrite the last equation as follows:

$$\begin{aligned} \dot{\tilde{x}}_n &= \tilde{x}^T\vartheta + [\vartheta - \hat{a}]^T x^d + \tilde{u} + [a - \vartheta]^T(\tilde{x} + x^d) \\ &= \psi^T(\tilde{x})\tilde{a} + \tilde{u}_2 \end{aligned}$$

where $\tilde{a} = a - \vartheta$, $\psi^T(\tilde{x}) = x^T$. Then $\sum_4$ is in a standard form with matching condition, then the goal becomes designing $\tilde{u}_2$ to guarantee the regulation of $\tilde{x}$. Details of the derivations are skipped here, but the final controller is given by:

$$u = u^d + \tilde{u}_2 - \tilde{x}^T\vartheta - [\vartheta - \hat{a}]^T x^d \tag{3.25}$$

$$\tilde{u}_2 = \alpha_n(\tilde{x}, \vartheta) \tag{3.26}$$

$$\dot{\vartheta} = \Gamma\psi z_n \tag{3.27}$$

where Γ is an adaptation gain matrix. The variables z_i and the stabilizing functions $\alpha_i, i = 1, \ldots, n$, are defined by the following recursive expressions:

$$z_i = \tilde{x}_i - \alpha_{i-1}(\tilde{x}_1, \ldots, \tilde{x}_{i-1}) \tag{3.28}$$

$$\alpha_i = c_i z_i - z_{i-1} + \sum_{j=1}^{i-1} \frac{\partial \alpha_{i-1}}{\partial \tilde{x}_j}\tilde{x}_{j+1}, \;\; i = 1, \cdots, n-1 \tag{3.29}$$

$$\alpha_n = c_n z_n - z_{n-1} - \psi^T\vartheta + \sum_{j=1}^{n-1} \frac{\partial \alpha_{n-1}}{\partial \tilde{x}_j}\tilde{x}_{j+1} \tag{3.30}$$

This adaptive controller guarantees global boundedness of $\tilde{x}(t), \vartheta(t)$, and regulation of $\tilde{x}_i(t), i = 1, \ldots, n$, i.e., $\tilde{x}_i(t) \to 0$, as $t \to \infty$.

3.3.3 Parameter Estimator

An off-line Least-Squares method is used to estimate the parameters. To get $\hat{a}_{k+1}$, we use the method as follows:

$$\hat{a}_{k+1} = d_k \hat{a}_k + (1 - d_k)\bar{a}_k \tag{3.31}$$

where $d_k \in [0, 1)$ is a memory factor and $\bar{a}_k$ is determined by using an off-line Least-Squares method [6]using data from the k^{th} trial. First using a filter for the last equation of $\sum_3$, we get

$$\frac{1}{s+\lambda}\dot{x}_n = \frac{1}{s+\lambda}x^T a + \frac{1}{s+\lambda}u \tag{3.32}$$

$$x_n - \frac{1}{s+\lambda}u = \frac{1}{s+\lambda}x^T \begin{pmatrix} a_0 \\ \vdots \\ a_{n-1} + \lambda \end{pmatrix} \tag{3.33}$$

where $\lambda > 0$. Then we have $Z = W^T \hat{a}_\lambda$, where $Z = (x_n - \frac{1}{s+\lambda}u)$, and $W^T = \frac{1}{s+\lambda}x^T$. By solving the ordinary differential equations (ODE), we get Z and W. Now collect all the data of Z and W. Suppose there are totally M samples for the k^{th} trial. Let $\Phi = [W_1^T, \cdots, W_M^T]^T$ and the regressor vector be $\Psi = [Z_1, \cdots, Z_M]^T$. The Least-Squares solution is

$$\hat{a}_\lambda = (\Phi^T \Phi)^{-1} \Phi^T \Psi \tag{3.34}$$

From this we get $\bar{a}_k$. Then $\hat{a}_{k+1}$ is obtained by (31). Similarly, for the linear model,

$$y = Cx \tag{3.35}$$

We can use the same argument to get the estimates of C, except that no filtering is needed.

3.3.4 Adaptive Learning Algorithm

The process of the algorithm is as follows:

Step 0 : Given ε, the initial conditions $\hat{a}_0$, $\hat{C}_0$, the initial input $u_0^d(t) = 0$, and initial state trajectory $x_0^d(t) = 0$ on $t \in [0, T]$, set k=0.

Step 1: Let $e_k(t) = y_d(t) - y_k(t)$. Get $\hat{G}_k$ from $\hat{a}_k$ and $\hat{C}_k$. Use stable inversion to get $u_{k+1}^e = \hat{H}_k e_k$ and x_{k+1}^e. Use equation (23) and (24) to get u_{k+1}^d and x_{k+1}^d.

Step 2: $u_{k+1}^d(t)$ is used as feed forward by the adaptive backstepping feedback controller to stabilize the system and to ensure regulation of $x_{k+1}^d(t)$, i.e., $x_k(t) \to x_{k+1}^d(t)$, as $t \to \infty$. The input and output trajectories are recorded respectively.

Step 3 : Then the tracking error signal $e_{k+1}(t)$ is calculated. If $\|e_{k+1}(\cdot)\|_\infty \leq \epsilon$, stops. Otherwise, set $k = k + 1$, and go to Step 4 .

Step 4: Use off-line Least-Squares method to obtain the parameter estimates $\hat{a}_k$ and $\hat{C}_k$, and go back to Step 1.

3.4 Simulation Illustrations

Simulation results are provided for SISO linear nonminimum phase systems with unknown parameters. Two examples of second order and third order unstable nonminimum phase systems are included to verify the effectiveness of the proposed adaptive learning algorithm.

Example 1 Consider a nonminimum phase plant:

$$\begin{cases} \dot{x}_1 = x_2 \\ \dot{x}_2 = [3 \quad 7]x + u \\ y = [10 \quad -1]x \end{cases}$$

The parameters $a = [3 \quad 7]^T$, $C = [10 \quad -1]$. This system has two poles at 7.4051, -0.4051, and one zero at 10. Take the initial conditions $\hat{a}_0 = [2.8 \quad 6.8]^T$, $\hat{C}_0 = [9 \quad -0.8]$. Let the desired trajectories $y_d(t) = 4.6685 - 0.4244cos(1.5708t) - 4.2441cos(0.1571t)$ as shown by the solid curve in Figure 2. Take an initial input $u_0^d(t) = 0$ and initial state trajectory $x_0^d(t) = 0$. Simulation results for the trial $k = 1$ and $k = 2$ are shown in Figure 3.2. At the 2^{nd} trial, the output $y_2(t)$ converges to the desired $y_d(t)$ exactly by the dotted curve. Table 3.1 shows the parameter estimates and the infinity norm of the

Table 3.1 Parameter estimates and output tracking error in each trial for the 2^{nd} order nonminimum phase system

k	$\hat{a}_{0,k}(3)$	$\hat{a}_{1,k}(7)$	$\hat{C}_{0,k}(10)$	$\hat{C}_{1,k}(-1)$	$\|e_k\|_\infty$
1	2.8999	6.9235	9.9999	-1.0000	0.1021
2	2.9339	6.9636	10.0000	-0.9999	0.0003
3	2.9510	6.9837	10.0000	-1.0000	0.0002
4	2.9609	6.9980	10.0000	-1.0000	0.0001

Table 3.2 Parameter estimates and output tracking error in each trial for 3^{rd} order nonminimum phase systems

k	$\hat{a}_{0,k}(1)$	$\hat{a}_{1,k}(2)$	$\hat{a}_{2,k}(3)$	$\hat{C}_{0,k}(-21)$	$\hat{C}_{1,k}(-4)$	$\hat{C}_{2,k}(1)$	$\|e_k(\cdot)\|_\infty$
k=1	0.8998	1.8982	2.9059	-21.0000	-4.0000	0.9999	0.1678
k=2	0.9332	1.9360	2.9391	-21.0000	-4.0000	1.0000	0.0007
k=3	0.9500	1.9541	2.9581	-21.0000	-3.9999	1.0000	0.0004
k=4	0.9600	1.9648	2.9671	-20.9999	-3.9999	1.0000	0.0002

output tracking error at each trial. We can see the estimated parameters are very close to the true values at the 3^{rd} trial.

Example 2 Consider a nonminimum phase plant:

$$\begin{cases} \dot{x}_1 = x_2 \\ \dot{x}_2 = x_3 \\ \dot{x}_3 = [1 \quad 2 \quad 3]x + u \\ y = [-21 \quad -4 \quad 1]x \end{cases}$$

The parameters $a = [1 \quad 2 \quad 3]^T, C = [-21 \quad -4 \quad 1]$. This system has poles at $-0.3137 \pm 0.4211i$, and 3.6274, and zeros at 7 and -3. Take initial conditions $\hat{a}_0 = [0.8 \quad 1.8 \quad 2.8]^T, \hat{C}_0 = [-25 \quad -3 \quad 2]$. Let the desired output $y_d(t) = -0.2759 - 0.0424cos(1.5708t) - 0.2122cos(0.3142t) - 0.1061cos(0.6283t)$ as shown by the solid curve in Figure 3. Take an initial input $u_0^d(t) = 0$ and initial state trajectory $x_0^d(t) = 0$. Simulation results for the trial $k = 1$ and $k = 2$ are shown in Figure 3.3. At the 2^{nd} trial, the output $y_2(t)$ converges to the desired $y_d(t)$ exactly as shown the dotted curve. Table 3.2

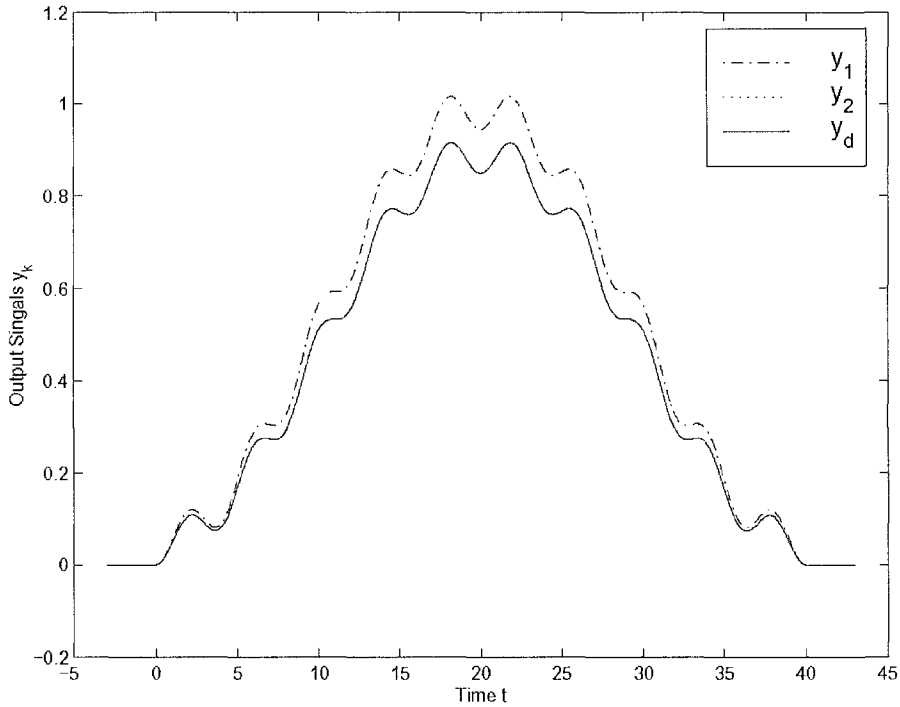

Figure 3.2 Tracking of 2^{nd} order linear nonminimum phase systems ($y_2(t)$ converges to $y_d(t)$ exactly)

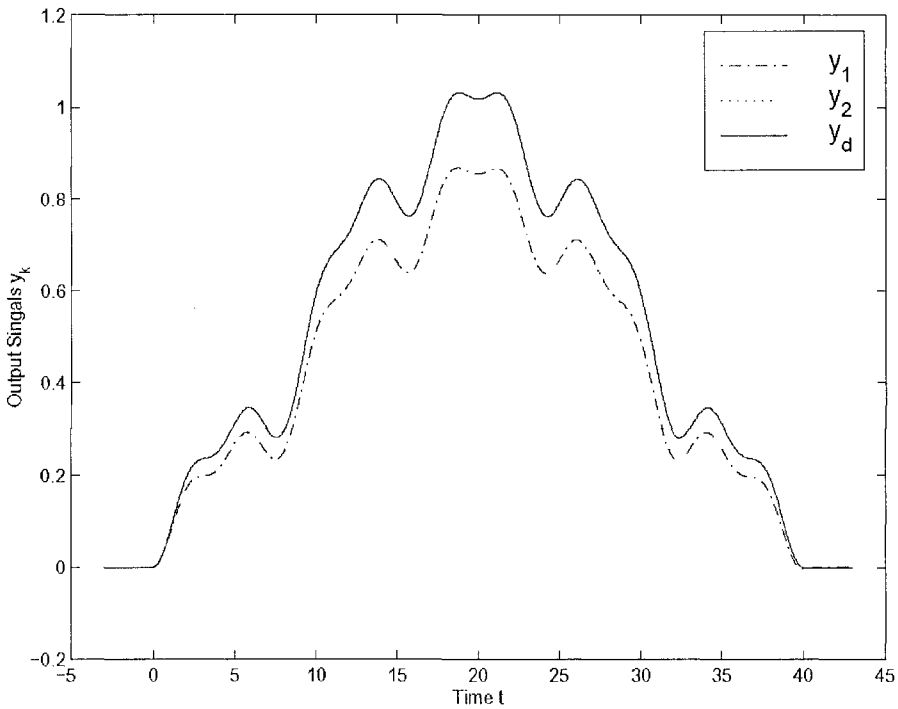

Figure 3.3 Tracking of 3^{rd} order linear nonminimum phase systems ($y_2(t)$ converges to $y_d(t)$ exactly)

shows the parameter estimates and the infinity norm of the output tracking error at each trial. We can see that the estimated parameters are very close to the true values at the 4^{th} trial.

The above results demonstrate that the proposed learning control is very effective in reproducing the desired trajectories.

3.5 Conclusions

A new adaptive learning algorithm has been developed for unstable nonminimum systems. The adaptive backstepping feedback control law is employed to guarantee regulation of tracking error and a stable inverse system is used to update the feed forward input for the next trial. Given a desired trajectory, the learning controller is able to learn and eventually drive the closed loop dynamics to track the desired trajectory. Simulation results demonstrate the effectiveness of the proposed method.

Bibliography

[1] S. Arimoto, S. Kawamura, and F. Miyazaki, "Bettering Operation of Robots by Learning," *Journal of Robotic Systems*, Vol. 1, pp. 123-140, 1984.

[2] P. Bondi, G. Casalino, and L. Gambardellal, "On the Iterative Learning Control Theory for Robotic Manipulators," *IEEE Transactions on Robotics and Automation*, Vol. 4, pp. 14-22, 1989.

[3] J. Gao and D. Chen, "Iterative Learning Control for Nonminimum Phase Systems," *American Control Conference*, 1998.

[4] D. Chen and B. Paden, "Stable Inversion of Nonminimum Phase Nonlinear Systems," *International Journal of Control*, Vol. 64, pp. 81-96, 1996.

[5] J. Hauser, "Learning Control for a Class Nonlinear Systems," *Proceedings of the 26th Conference on Decision and Control*, pp. 859-860, 1987.

[6] R. Johansson, *System Modelling Identification,* Prentice Hall, Englewood Cliffs, New Jersey, 1993.

[7] S. Kawamura, F. Miyazaki, and S. Arimoto, "Application of Learning Method for Dynamic Control of Robot Manipulations," *Proceedings of the 24th Conference on Decision and Control*, 1381-1386, 1985.

[8] M. Krstić, I. Kanellakopoulos, and P. V. Kokotovic, *Nonlinear and Adaptive Control Design,* Wiley, New York, 1995.

[9] K. Moore, *Iterative Learning Control for Deterministic Systems,* Springer-Verlag, New York, 1993.

[10] K. Moore, M. Daleh, and S. Bhattacharya, "Iterative Learning Control: A Survey and New Results," *Journal of Robotic Systems,* Vol. 9, pp. 563-594, 1992.

4 Robust Inversion-based Learning Control for Nonminimum Phase Systems

Abstract — This paper introduces a new robust inversion-based learning algorithm for the repetitive tracking control of a class of unstable nonminimum phase systems. After each repetitive trial, the Least-Squares method is used to estimate the system parameters. The output tracking error and the identified system model are used through stable inversion to find the feed forward input, together with the desired state trajectories, for the next trial. A robust controller is used in each trial to ensure the stability of the systems and the output tracking error convergence. Sufficient conditions for learning control convergence are provided. Simulation studies on the systems with gain uncertainty and time constant uncertainty are also presented. In addition, simulation results demonstrate that the proposed learning control scheme is very effective in reproducing the desired trajectories.

4.1 Introduction

Iterative learning control (ILC) is a feed forward control approach aimed at achieving high performance output tracking control by "learning" from past experience so as to eliminate the repetitive errors from future execution [4]. This approach was motivated by the observation that humans are able to improve their performance through repeated practice.

The concept of iterative learning for generating the optimal input to a system was first introduced by Uchiyama [1] to improve the performance of robot motion. Later the idea was developed by a research group headed by Suguru Arimoto. He and his

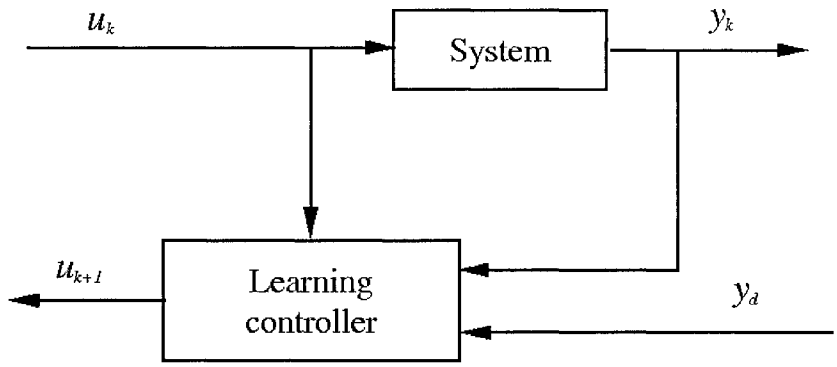

Figure 4.1 Learning control system

colleagues began publishing their work for repetitive robot control [5, 6], which led to increased interest in ILC, particularly through the middle to late 1980's. The work was based on using repeated trials to track a desired trajectory.

The basic idea of the approach is illustrated by Figure 4.1. During each trial, the system input and output signals are stored. The learning control algorithm then evaluates the performance error. Based on the error signal, the learning controller computes a new input signal, which is stored for use during the next trial. The new input is chosen such that the performance error will be reduced in the next trial. The "learning" action is done "off-line" between two consecutive trials and uses the entire error history from the previous trial to modify the entire input signal for the next trial. One of the important features of ILC is that it requires little *a priori* knowledge about the controlled system during the controller design phase. More importantly, the learning process provides a system with the ability to "learn" to improve its performance.

For linear systems, Arimoto *et al.* [5] first proposed a learning control method for linear time-varying, continuous-time systems. It assumes that the system relative degree is one. It was shown that y_k will eventually match y_d exactly as the number of trials increases under certain conditions. This algorithm is called a D-type algorithm since the derivative of the output error is used to update the next input. Arimoto [6] modified the above algorithm and considered P-type and PD-type learning controllers. Moore

[4] modified the Arimoto method and extended it to systems with relative degree larger than one. Furuta and Yamakita [7] presented a modification of Moore's method. A proportional (P) learning algorithm was used, with respect to a specific function of output error instead of with simple output error. Their algorithm provided convergence in the sense of the L_2 norm but required the complete knowledge of the adjoint system, which is equivalent to needing the complete knowledge of the system dynamics.

Hauser presented a nonlinear version of Arimoto's method for a class of nonlinear systems [19] and provided sufficient conditions for its uniform convergence. Hauser's method is more general than Arimoto's method. For a more specific structure, Sugie and Ono [8] provided the learning controller given by a linear time-varying system and showed its convergence under some conditions. Kuc *et al.* [9] presented an ILC scheme for a class of nonlinear dynamic systems. They suggested an ILC scheme with high-gain feedback PD controller, which updated the feed forward control input with the feedback controller output. Saab [13] presented sufficient conditions for the convergence of a P-type learning algorithm for a class of time-varying, nonlinear systems. Jang *et al.* [10] proposed an ILC method to achieve precise tracking control of a class of nonlinear systems. The learning was done in a feedback configuration and the learning law updated the feedforward input from the plant input of the previous trial. It was shown that the feedback controller had no effect on the convergence condition of the learning control while it could significantly improve the performance of learning. Comprehensive analysis, design, and applications of ILC could be found from [4, 11, 12].

Although existing learning algorithms have been theoretically proven to provide output error convergence with successful applications, many such algorithms have practical difficulties with nonminimum phase systems. Amann and Owens [2] showed that a zero of the plant in the RHP caused very slow convergence of the input sequence and resulted in a nonzero error for some iterative control algorithms. Gao and Chen [14] illustrated with counter-examples the limitations of some of the existing learning algorithms with regard to nonminimum phase systems. To remove the minimum phase requirement, they developed a new adaptive learning algorithm for stable linear systems based on "stable

inversion". Based on the algorithm of Gao and Chen, Ghosh and Paden [15, 16] developed an ILC algorithm for nonlinear nonminimum phase plants with input disturbances and output sensor noise. An extension to the ILC algorithm in [15, 16] was presented [17] so that it could be applied to a nonminimum phase plant with neglected and unmodeled dynamics. All the algorithms developed by Ghosh and Paden assume that the plants are stable and assume the system parameter are known. Wang and Chen [21] presented an adaptive learning control algorithm for unstable nonminimum phase systems. In this paper, a robust learning algorithm that can guarantee the learning control convergence is developed to work for unstable nonminimum phase systems. Simulation studies are presented to show the effectiveness of the proposed robust learning algorithm.

The remainder of this paper is organized as follows: In the next section, a class of desired trajectories under consideration is defined and the problem of ILC is stated. The learning control convergence issue is also addressed. Section 4.3 presents the new robust learning control law and a sufficient condition for the convergence property of the proposed ILC. Section 4.4 applies the proposed robust ILC to linear systems with gain uncertainty and time constant uncertainty. Section 4.5 shows the simulation results for these two types of linear systems. Finally, some conclusions are given in Section 4.6.

4.2 Framework and Problem Statement

Consider a nonlinear time varying plant model in the k^{th} trial:

$$y_k(t) = \Phi(x_k(t), \theta, u_k(t)) \tag{4.1}$$

where, for all $t \in [0, T]$, $x_k(t) \in \Re^n$, $u_k(t) \in \Re^m$, $y_k(t) \in \Re^p$. And θ is a parameter vector.

In addition, we make the following assumptions:

(A1) The system has a well-defined relative degree $r = (r_1, \cdots, r_m)^T$ that is known. The linearization of the system about an equilibrium point, which is assumed to be the origin WLOG, is completely controllable.

(A2) The order of the system, n, is known.

(A3) The system parameter vector θ is unknown or known incompletely.

(A4) A desired output trajectory is given and is a sufficiently smooth function of t satisfying $y_d(t) = 0$ for any $t \in (-\infty, 0] \cup [T, \infty)$ and finite for any $t \in (0, T)$, where $T > 0$.

(A5) The system can be represented in terms of control input $u_k(\cdot)$ and output $y_k(\cdot)$ in the k^{th} trial by means of a nonlinear time-varying operator Φ as follows:

$$y_k(\cdot) = \Phi\{u_k(\cdot)\} \tag{4.2}$$

The operator $\Phi\{\cdot\}$ is uniformly globally Lipschitz in u_k on the interval $[0, T]$. That is, $\|\Phi u_k - \Phi u_{k+1}\| \leq L\|u_k(t) - u_{k+1}(t)\|, \ \forall t \in [0, T]$ with a Lipschitz constant $0 \leq L < \infty$.

Iterative Learning Control Problems :

Given a desired output trajectory $y_d(t)$ and a tolerance error bound ϵ for a class of system (1) and (2), starting from an arbitrary continuous initial control input $u_0^d(\cdot)$ and initial state $x_0^d(\cdot)$, iterative learning control will try to find a sequence of desired state trajectories $x_k^d(\cdot)$ and desired control inputs $u_k^d(\cdot)$, which when applied to the system, produces an output sequence $y_k(\cdot)$ such that

(1) $\|y_d(\cdot) - y_k(\cdot)\|_\infty \leq \epsilon$, as $k \to \infty$, where k is the trial number and $\|f\|_\infty = \sup_{t\in[0,T]}\|f(t)\|$.

(2) $\|u_k^d(t)\| \leq \epsilon, \|x_k^d(t)\| \leq \epsilon, \forall t \in (-\infty, 0] \cup [T, +\infty)$.

(3) $u_k^d(t)$, $x_k^d(t)$, $u_k(t)$, and $x_k(t)$ are uniformly bounded.

In this dynamic process, the functions have two arguments: continuous time t and the trial number k. In the sequel, it is assumed that the variation of the operator over two consecutive trials is slow and can be neglected. Then the operator obtained by the identification performed in the k^{th} trial can be used to determine the input for the $(k+1)^{th}$ trial. This general description of the problem allows a simultaneous description of linear or nonlinear dynamics, continuous or discrete plant, and time-invariant or time-varying systems.

When applying a linear ILC, however, the plant must fulfill the following conditions: (1) The desired trajectory $y_d(t)$ is identical for every trial and satisfies Assumption (A4). (2) Each trial has the fixed period T. (3) The system parameters are fixed or very slowly time-varying.

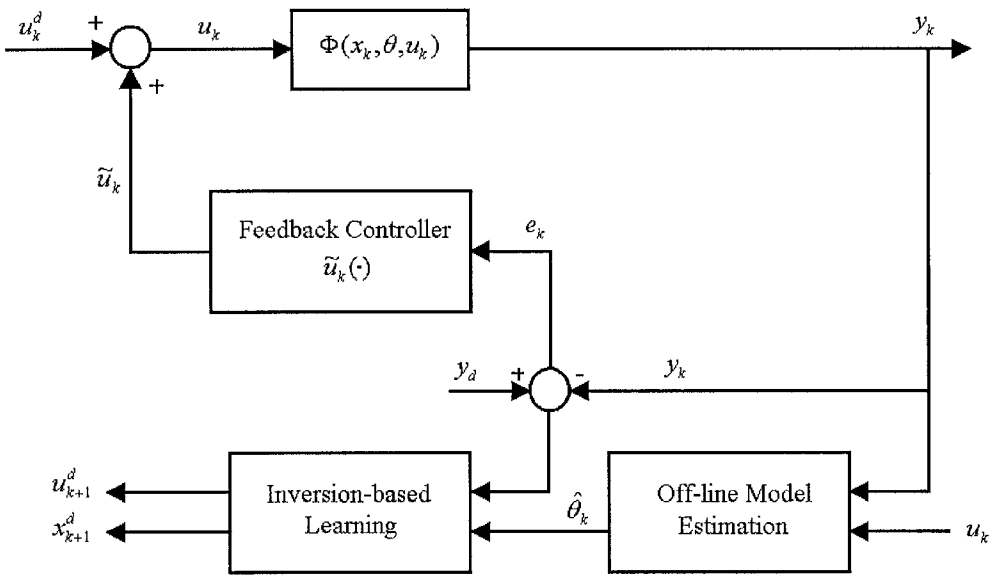

Figure 4.2 Block diagram of inversion-based learning control system

At any trial k, define a tracking error to be $e_k = y_d - y_k$. Learning control convergence means that $\|e_k\| \to 0$ as $k \to \infty$. The λ-norm defined in Arimoto *et al.* [5] has been adopted in many papers [4] as the topological measure in the proof of the convergence property for a newly proposed ILC. The formal definition [5] of the λ-norm for a function $f : [0, T] \to \Re^n$ is given by

$$\|f(\cdot)\|_\lambda \triangleq \sup_{t\in[0,T]} e^{-\lambda t}\|f(t)\| \tag{4.3}$$

It is easily observed that $\|f\|_\lambda \leq \|f\|_\infty \leq e^{\lambda T}\|f\|_\lambda$ for $\lambda > 0$, where $\|f\|_\infty \triangleq \sup \|f(t)\|_\infty$, implying the $\lambda-$norm is equivalent to the sup norm.

4.3 Inversion-Based Learning Controller Design

In Section 4.2, we have given the general setup for learning control. In this section, a robust learning controller will be presented. The block diagram of the robust learning system is shown in Figure 4.2.

The proposed robust learning control strategy has three components: a parameter

estimator, a stable inverse system, and a robust feedback controller. The parameter estimator is in charge of "learning" the parameterized model of the system. During each trial, the input and output trajectories are recorded. Then an off-line Least-Squares method [20] is applied to obtain the optimal estimate of parameters. Also obtained during each trial is the output tracking error signal. This error signal and the estimated model are used by the stable inverse system to learn the optimal input signal for the next trial. Although the estimated model may be nonminimum phase which normally leads to unbounded inverse solutions, stable inversion guarantees a unique and bounded inverse solution. This "learning" action is done "off-line" between two consecutive trials. Afterwards, the new feed forward input is used by a feedback controller to stabilize the system and to ensure regulation of the tracking error. The same feedback control algorithm is used during every trial.

In the following, sufficient conditions of learning convergence for linear systems are to be addressed. The stable inversion solution to nonminimum phase systems is provided as well.

4.3.1 Sufficient condition of learning convergence for linear systems

One of the advantages for linear systems is that one can obtain an explicit relation between $\|e_{k+1}\|_\infty$ and $\|e_k\|_\infty$.

For LTI systems, the learning control update law is chosen as

$$u^d_{k+1} = u^d_k + \hat{H}_k e_k$$

where $\hat{H}_k$ is a linear operator.

A fixed controller K could be chosen. Thus, the output tracking error is described as follows:

$$\begin{aligned} e_{k+1} &= y_d - y_{k+1} \\ &= e_k + Gu_k - Gu_{k+1} \end{aligned}$$

Since $u_k = \tilde{u}_k + u_k^d$ and $\tilde{u}_k = Ke_k$, we have

$$\begin{aligned} e_{k+1} &= e_k + G(\tilde{u}_k + u_k^d) - G(\tilde{u}_{k+1} + u_{k+1}^d) \\ &= e_k - G(u_{k+1}^d - u_k^d) + G(\tilde{u}_k - \tilde{u}_{k+1}) \\ &= e_k - G\hat{H}_k e_k + G(Ke_k - Ke_{k+1} \\ &= (I - G\hat{H}_k)e_k + G(Ke_k - Ke_{k+1}) \\ &= (I + GK - G\hat{H}_k)e_k - GKe_{k+1} \end{aligned}$$

it yields

$$\begin{aligned} e_{k+1} &= (I + GK)^{-1}(I + GK - G\hat{H}_k)e_k \\ &= I - (I + GK)^{-1}G\hat{H}_k)e_k \end{aligned}$$

Furthermore, taking the norms yields

$$\|e_{k+1}\|_\infty = \|I - (I + GK)^{-1}G\hat{H}_k)\|_\infty \|e_k\|_\infty$$

Then the sufficient condition for learning convergence is

$$\|I - (I + GK)^{-1}G\hat{H}_k)\|_\infty \leq \rho < 1 \tag{4.4}$$

with $\rho \in (0, 1)$.

There are several options for choosing $\hat{H}_k$ and controller K. Among these options, $\hat{H}_k$ can be selected as the stable inverse of $(I + \hat{G}_k K)^{-1}\hat{G}_k$, where $\hat{G}_k$ is the estimated model of the system for trial k and K can be chosen as a robust controller if the systems have some uncertainties.

In the following section, a solution to stable inversion of linear nonminimum phase systems is presented.

4.3.2 Solution to stable inversion of nonminimum phase systems

Consider a LTI system in the form:

$$\sum\nolimits_1 : \begin{cases} \dot{x} = Ax + Bu \\ y = Cx + Du \end{cases}$$

If $\hat{G}$ is nonminimum phase, this will lead to unbounded solutions. The stable inversion theory [18] provides an avenue to overcome this difficulty. The procedure to obtain a unique stable inverse solution $u^d = \hat{H}y_d$ is illustrated below. There are four steps:

(1) Find the time-domain state-space model of $\hat{G}$:

Since $\hat{G}u^d = \hat{G}\hat{H}y_d = y_d$, a state-space representation of $\hat{G}$ yields

$$\dot{x}^d(t) = \hat{A}x^d(t) + \hat{B}u^d(t) \tag{4.5}$$

$$y_d(t) = \hat{C}x^d(t) + \hat{D}u^d(t) \tag{4.6}$$

where x^d is the state and $\hat{A}, \hat{B}, \hat{C}$, and $\hat{D}$ are matrices with suitable sizes.

(2) Find its inverse in state space:

Differentiate $y_d(t)$ until u^d appears explicitly in the right hand side. Solve for u^d and substitute into (4.5) and (4.6) to obtain

$$\dot{x}^d(t) = \bar{A}x^d(t) + \bar{B}y_d^{(r)}(t) \tag{4.7}$$

$$u^d(t) = \bar{C}x^d(t) + \bar{D}y_d^{(r)}(t) \tag{4.8}$$

where $\bar{A}, \bar{B}, \bar{C}$, and $\bar{D}$ are defined according to the substitution.

(3) Decompose the inverse system into center, stable, and unstable subsystems:

Perform a change of variables so that

$$x^d = Pz = P[z^c, z^s, z^u]^T \tag{4.9}$$

which leads to

$$\dot{z}^c = A^c z^c + B^c y_d^{(r)} \tag{4.10}$$

$$\dot{z}^s = A^s z^s + B^s y_d^{(r)} \tag{4.11}$$

$$\dot{z}^u = A^u z^u + B^u y_d^{(r)} \tag{4.12}$$

$$u^d = [C^c \;\; C^s \;\; C^u][z^c \;\; z^s \;\; z^u]^T + \bar{D}y_d^{(r)} \tag{4.13}$$

where A^c, A^s, and A^u are real Jordan matrices of suitable dimensions; A^c has r eigenvalues at zero; A^s has all eigenvalues in the open left-half plane; A^u has all eigenvalues in the open right-half plane.

(4) Obtain the stable inverse system:

Pick the transformation matrix P so that the center subsystem is a simple chain of r integrators. Solve that and impose two boundary conditions on the stable and unstable subsystems to yield

$$z^c = [y_d, \dot{y}_d, \cdots, y_d^{(r-1)}]^T \tag{4.14}$$

$$\dot{z}^s = A^s z^s + B^s y_d^{(r)}, t \geq 0; z^s(t) = 0, \quad \forall\, t \leq 0 \tag{4.15}$$

$$\dot{z}^u = A^u z^u + B^u y_d^{(r)}, t \leq T; z^u(t) = 0, \quad \forall\, t \geq T \tag{4.16}$$

These together with (4.9) and (4.13) define the desired stable inverse system.

The stable inverse system always yields bounded solutions for bounded and smooth y_d. This can be clearly seen from (4.14, 4.15, 4.16) since the center solution z^c is clearly bounded, the stable subsystem is in the forward time, and the unstable subsystem is in the reverse time, all leading to bounded solutions.

4.3.3 Inversion-based learning

Based on the stable solutions outline presented above, to facilitate iterative learning, the inversion process is slightly modified as follows.

Since G is unknown and $\hat{G}_k$ is the best estimate model after the k^{th} trial, one would select

$$u_{k+1}^e = \hat{H}_k e_k \tag{4.17}$$

$$x_{k+1}^e = P_k z = P_k [z^c, z^s, z^u]^T \tag{4.18}$$

so that $e_k = \hat{G}_k u_{k+1}^e$. Then the learning algorithm becomes

$$u_{k+1}^d = u_k^d + u_{k+1}^e \tag{4.19}$$

There are various methods to design the feedback controller. For systems with uncertainties, a robust controller will be chosen to stabilize the systems.

In the following section, the implementation of the robust learning algorithm for two types of LTI systems is presented.

4.4 Learning Control of Linear Systems with Uncerntainty

Sufficient conditions for learning control convergence for linear systems with gain uncertainty and time constants uncertainty are provided in this section.

4.4.1 Learning Control of Systems with Gain Uncertainty

In this section, the following type of linear nonminimum phase system with gain uncertainty is considered. Let the set of possible plants be

$$G_p(s) = k_p G_0(s), \qquad k_{min} < k_p < k_{max}$$

where $G_0(s) = \frac{s-z}{s^2+as+b}$ with $z > 0, a < 0, b > 0$, and $b \geq -az$.

For the above system, the uncertainty can be expressed as the following multiplicative uncertainty: $G_p(s) = \bar{k}_p(1+r\Delta)G_0(s) \quad |\Delta| \leq 1$ where $\bar{k}_p = \frac{k_{max}+k_{min}}{2}$ and $r = \frac{k_{max}-k_{min}}{k_{max}+k_{min}}$.

The closed-loop transfer function is given as

$$\frac{k_p(s-z)}{s^2+(a+k_pK)s+b-k_pKz}$$

To guarantee the stability of the system, the following inequalities should be satisfied:

$$\begin{cases} k_pKz > -az \\ k_pKz < b \end{cases}$$

The robust controller can be chosen as

$$K = \frac{\sqrt{-abz}}{\bar{k}_p z} \tag{4.20}$$

which means

$$\begin{cases} \sqrt{-abz}(1-r) > -az \\ \sqrt{-abz}(1+r) < b \end{cases}$$

Thus, to guarantee the stability, r should satisfy

$$r < \min(1 + \frac{az}{\sqrt{-abz}}, \frac{b}{\sqrt{-abz}} - 1) \tag{4.21}$$

For a specific example, setting $a = -1, z = 3, b = 12, k_{min} = 0$, and $k_{max} = 4$, the following system is considered

$$G_p(s) = k_p \frac{s-3}{s^2-s+12}, \qquad 0 < k_p < 4 \tag{4.22}$$

where $k_p = 2.15$.

This system has a zero at 3, and has poles at $0.5 \pm 3.4278i$. The causal reference output trajectory is given by:

$$y_d = \begin{cases} 5 - 5\cos(0.4\pi t), & t \in [0, 5] \\ 0, & \text{otherwise} \end{cases}$$

as shown by the solid curve in Figure 4.3. Then by (4.21), to guarantee the systems stability, r should satisfy $r < 0.5$.

If $\hat{H}_k$ is chosen as the stable inverse of $(I + \hat{G}_p K)^{-1}\hat{G}_p$, then by (4.4) and (4.20), to guarantee the learning convergence, the following condition should be satisfied,

$$\begin{aligned} & \|1 - (1 + G_p K)^{-1} G_p \hat{H}_k\|_\infty \\ &= \|1 - \frac{k_p(s-3)}{s^2 - s + 12 + K k_p (s-3)} \frac{s^2 - s + 12 + K\hat{k}_p(s-3)}{\hat{k}_p(s-3)}\|_\infty \\ &= \|1 - \frac{k_p}{\hat{k}_p} - \frac{k_p K(\hat{k}_p - k_p)}{\hat{k}_p} \frac{s-3}{s^2 - s + 12 + K\hat{k}_p(s-3)}\|_\infty \\ &\leq 2r + 4r(1+r)\|\frac{s-3}{s^2 - s + 12 + K\hat{k}_p(s-3)}\|_\infty \\ &\leq \rho < 1 \end{aligned}$$

Hence the range for r to guarantee the learning convergence is $r \in [0, 0.092]$. Combined with $r < 0.5$, to guarantee both the learning convergence and the stability of the system, r should satisfy $r \in [0, 0.092]$. Thus $\hat{k}_p \in [\bar{k}(1-r), \bar{k}(1+r)]$, i.e., $\hat{k}_p \in [1.816, 2.184]$, which means the estimated parameter $\hat{k}_p$ should be restricted in the above range in order to guarantee the learning convergence.

4.4.2 Learning Control of Systems with Time Constant Uncertainty

In this section, the following single-input single-output linear nonminimum phase system with time constant uncertainty is considered. Let a set of plants are given by

$$G_p(s) = \frac{G_0(s)}{\tau_p s + 1}, \qquad \tau_{min} < \tau_p < \tau_{max}$$

where $G_0(s) = \frac{s-z}{s-p}$ with $z - p \geq \frac{\tau_{max} + \tau_{min}}{2} pz > 0$ and $\tau_{min} \geq 0$. For the above system, the uncertainty can be expressed as the following inverse multiplicative uncertainty:

$G_p(s) = \frac{G_0(s)}{\bar{\tau}(1+r\Delta)}$ $|\Delta| \leq 1$ where $\bar{\tau} = \frac{\tau_{max}+\tau_{min}}{2}$ and $r = \frac{\tau_{max}-\tau_{min}}{\tau_{max}+\tau_{min}}$. The closed-loop transfer function is given as

$$\frac{\frac{s-z}{\tau_p s^2+(1-\tau_p p+K)s-p-Kz}}{}$$

To guarantee the stability of the system, the following inequalities should be satisfied:

$$\begin{cases} k_p K z > -az \\ k_p K z < b \end{cases}$$

The robust controller can be chosen as

$$K = -\frac{\sqrt{pz[1-\bar{\tau}(1+r)p]}}{z} \tag{4.23}$$

Then it yields

$$\begin{cases} r < \frac{z-p}{\bar{\tau}pz} - 1 \\ 1 - \bar{\tau}(1+r)p > 0 \end{cases}$$

Thus, to guarantee the stability, r should satisfy

$$r < \min(\frac{z-p}{\bar{\tau}pz} - 1, \frac{1}{\bar{\tau}p} - 1) \tag{4.24}$$

For a specific example, setting $z = 4, p = 1, k_{min} = 0$, and $k_{max} = 1$, the following system is considered

$$y = \frac{s-4}{(\tau_p s+1)(s-1)}u, \qquad 0 < \tau_p < 1 \tag{4.25}$$

where $\tau_p = 0.473$. This system has a zero at 4, and has poles at -2.1142 and 1. The causal reference output trajectory is given by:

$$y_d = \begin{cases} 10 - 10\cos(0.2\pi t), & t \in [0, 10] \\ 0, & \text{otherwise} \end{cases}$$

as shown by the solid curve in Figure 4.6.

Then by (4.24), to guarantee the systems stability, r should satisfy

$$r < 0.5 \tag{4.26}$$

If $\hat{H}_k$ is chosen as the stable inverse of $(I + \hat{G}_p K)^{-1}\hat{G}_p$, then by (4.4) and (4.23), to guarantee the learning convergence, the following condition should be satisfied,

$$\begin{aligned}
&\|1 - (1 + G_p K)^{-1} G_p \hat{H}_k\|_\infty \\
&= \|1 - \frac{s-4}{(\tau_p s+1)(s-p)+K(s-4)} \frac{(\hat{\tau_p} s+1)(s-p)+K(s-4)}{s-4}\|_\infty \\
&= \|1 - \frac{\hat{\tau_p}}{\tau_p} - (1 - \frac{\hat{\tau_p}}{\tau_p}) \frac{(1+K)s-1-4K}{(\tau_p s+1)(s-1)+K(s-4)}\|_\infty \\
&\leq 2r + 2r\|\frac{(1+K)s-1-4K}{(\tau_p s+1)(s-1)+K(s-4)}\|_\infty \\
&\leq \rho < 1
\end{aligned}$$

Thus the range for r to guarantee the learning convergence is $r \in [0, 0.273]$. Combined with (4.26), to guarantee both the learning convergence and the stability of the system, r should satisfy $r \in [0, 0.273]$. Hence $\hat{\tau}_p \in [\bar{\tau}(1-r), \bar{\tau}(1+r)]$, i.e., $\hat{\tau}_p \in [0.3635, 0.6365]$, which means the estimated parameter $\hat{\tau}_p$ should be restricted in the above range in order to guarantee the learning convergence.

4.5 Simulation results

In this section, two specific examples (4.22) and (4.25) are simulated. Here, suppose only output and input signals can be measured. In addition, there is random noise on output measurements, which has mean 0 and deviation 0.01.

For each of two examples, three cases are simulated. For all three cases, the least-squares method is used to estimate the unknown parameter. For Case 1, take the initial condition within the range. The estimated parameter is always enforced within the range by projection. For Case 2, take the initial condition beyond the range. The estimated parameter is used without projection. For Case 3, take the initial condition beyond the range. The estimated parameter is always enforced outside the range.

The initial conditions of the unknown parameters for these two examples are shown in the following table:

Given an initial input $u_0^d(t) = 0$, simulation results for the trial $k = 1$ and $k = 2$ are shown in Figure(4.3-4.5) for Example 1 and shown in Figure(4.6-4.8) for Example 2.

For both two examples, at the 2^{nd} trial, the output $y_2(t)$ converges to the desired $y_d(t)$ exactly shown by the dotted curve for Case 1 and Case 2. But the output $y_2(t)$

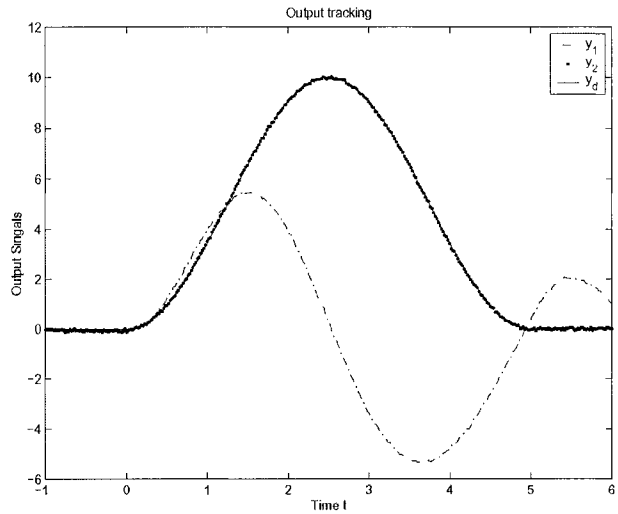

Figure 4.3 Tracking of nonminimum phase systems with gain uncertainty for Case 1 ($y_2(t)$ converges to $y_d(t)$ exactly)

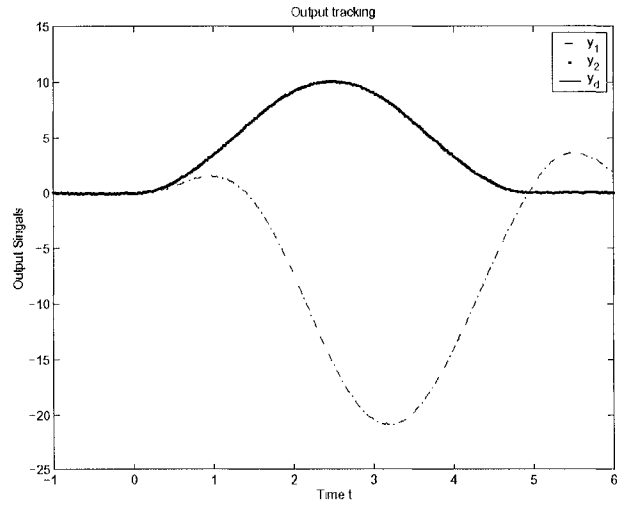

Figure 4.4 Tracking of nonminimum phase systems with gain uncertainty for Case 2 ($y_2(t)$ converges to $y_d(t)$ exactly)

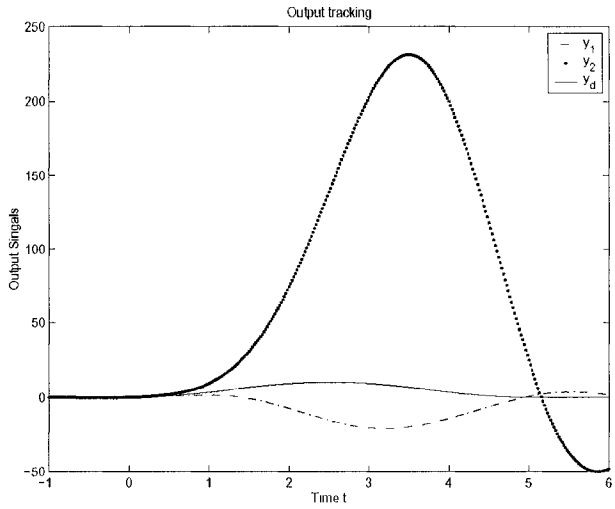

Figure 4.5 Tracking of nonminimum phase systems with gain uncertainty for Case 3 ($y_2(t)$ converges to $y_d(t)$ exactly)

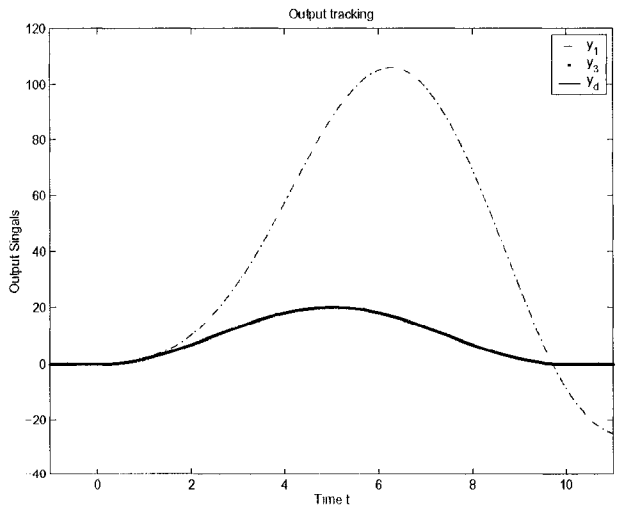

Figure 4.6 Tracking of nonminimum phase systems with time constant uncertainty for Case 1 ($y_3(t)$ converges to $y_d(t)$ exactly)

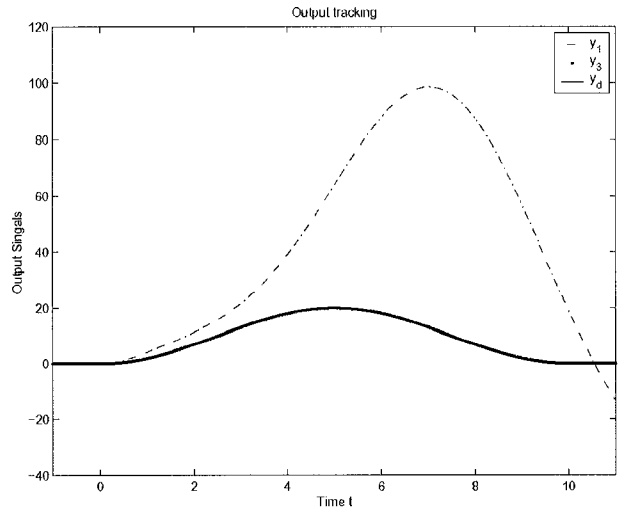

Figure 4.7 Tracking of nonminimum phase systems with time constant uncertainty for Case 2 ($y_3(t)$ converges to $y_d(t)$ exactly)

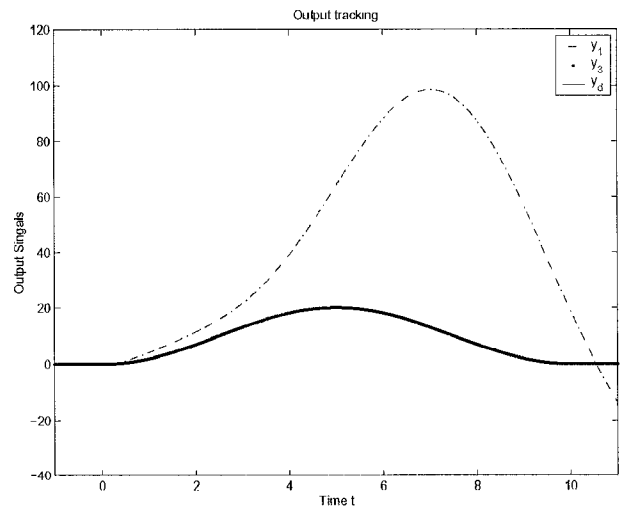

Figure 4.8 Tracking of nonminimum phase systems with time constant uncertainty for Case 3 ($y_3(t)$ converges to $y_d(t)$ exactly)

Table 4.1 Initial condition of the unknown parameters for two examples

	Example 1($\hat{k}_p$)	*Example* 2($\hat{\tau}_p$)
Case 1	1.98	0.6
Case 2	6	1.5
Case 3	6	1.5

Table 4.2 Output tracking error of nonminimum phase systems with gain uncertainty

k	*Case* 1	*Case* 2	*Case* 3
1	12.6169	29.4802	29.4802
2	0.1238	0.1908	225
3	0.1233	0.1446	1662
4	0.1106	0.1267	12334

diverges tremendously for Case 3. Table 4.2 and Table 4.3 shows the infinity norm of the output tracking error at each trial for three cases for Example 1 and Example 2 respectively. The infinity norm of the output tracking error decreases for Case 1 and Case 2, while it increases largely for Case 3.

The above results demonstrate that the proposed learning control is very effective in reproducing the desired trajectories. Simulation results also show that the provided condition is only a sufficient condition not a necessary condition.

Table 4.3 Output tracking error of nonminimum phase systems with time constant uncertainty

k	*Case* 1	*Case* 2	*Case* 3
1	89.5941	86.4392	86
2	0.6494	0.6407	710
3	0.0391	0.0260	5813
4	0.0159	0.0173	56337

4.6 Conclusions

A new inversion-based robust learning algorithm has been developed for unstable nonminimum phase systems. The sufficient condition for the convergence of the proposed ILC is also provided. The robust feedback control law is employed to guarantee the system stability and the convergence of tracking error, and a stable inverse system is used to update the feed forward input for the next trial. Simulation studies on two types of linear systems with gain uncertainty and time constant uncertainty are presented. Given a desired trajectory, the learning controller is able to learn and eventually drive the closed-loop dynamics to track the desired trajectory. Simulation results demonstrate the effectiveness of the proposed method.

Bibliography

[1] M. Uchiyama, "Formation of high speed motion pattern of mechanical arm by trial," *Transactions of the Society of Instrumentation and Control Engineers*, Vol. 19, pp. 706-712, 1978.

[2] N. Amann, D. H. Owens, and E. Rogers, "Non-minimum phase plant in iterative learning control," *Proceedings of the 2th Conference on Intelligent System Engineering*, pp. 107-112, 1994.

[3] N. Amann, D. H. Owens, and E. Rogers, "New results in iterative learning control," *IEE Proceedings Conference on CONTROL'94*, No. 389, pp. 640-645, 1994.

[4] K. L. Moore, *Iterative learning control for deterministic systems*, Springer-Verlag, New York, 1993.

[5] S. Arimoto, S. Kawamura, and F. Miyazaki, "Bettering operation of robots by learning," *Journal of Robotic Systems*, Vol. 1, pp. 123-140, 1984.

[6] S. Arimoto, S. Kawamura, F. Miyazaki, and S. Tamaki, "Learning control theory for dynamical systems," *Proceedings of the 24th Conference on Decision and Control*, pp. 1375-1380, 1985.

[7] K. Furuta and M. Yamakita, "The design of a learning control system for multivariable systems," *Proceedings of IEEE International Symposium on Intelligent Control*, pp. 371-376, 1987.

[8] T. Sugie and T. Ono, "An iterative learning control law for dynamical systems," *Automatica*, Vol. 27, pp. 729-732, 1991.

[9] J. E. Kuc and M. B. Zaremba, "An iterative learning control theory for a class of nonlinear dynamics systems," *Automatica*, Vol. 28, pp. 1215-1221, 1992.

[10] T. J. Jang and C. H. Ahn, "Iterative learning control in feedback systems," *Automatica*, Vol. 31, pp. 243-248, 1995.

[11] Z. Bien and J. X. Xu, *Iterative learning control*, Kluwer Academic Publishers, 1998.

[12] Y. Chen and C. Wen, *Iterative learning control*, Springer, 1999.

[13] S. Saab, "On the P-type learning control," *IEEE Transactions on Automatic Control*, Vol. 39, pp. 2298-2302, 1994.

[14] J. Gao and D. J. Chen, "Iterative learning control for nonminimum phase systems," *American Control Conference*, 1998.

[15] J. Ghosh and B. Paden, "Iterative learning control for nonlinear nonminimum phase plants with input disturbances," *American Control Conference*, Vol. 4, pp. 2584-2589, 1999.

[16] J. Ghosh and B. Paden, "Pseudo-inverse based Iterative Learning Control for Nonlinear Plants with Disturbances," *Proceedings of the 38th IEEE Conference on Decision and Control*, Vol. 5, pp. 5206-5212, 1999.

[17] J. Ghosh and B. Paden, "Pseudo-inverse based Iterative Learning Control for Plants with Unmodelleds Dynamics," *Proceedings of the 2000 American Control Conference*, Vol. 1, pp. 472-476, 2000.

[18] D. Chen and B. Paden, "Stable inversion of nonminimum phase nonlinear systems," *International Journal of Control*, Vol. 64, pp. 81-96, 1996.

[19] J. Hauser, "Learning control for a class nonlinear systems," *Proceedings of the 26th Conference on Decision and Control*, pp. 859-860, 1987.

[20] R. Johansson, *System Modelling Identification,* Prentice Hall, Englewood Cliffs, New Jersey, 1993.

[21] X. Z. Wang and D. J. Chen, "Adaptive learning control for nonminimum phase systems," *2000 IEEE International Conference on Systems, Man, and Cybernetics*, Vol. 1, pp. 26-31, 2000.

5 Design of a CMOS Low Noise Amplifier (LNA) at 5.8 GHz and Its Sensitivity Analysis

Abstract — This paper presents a 5.8 GHz low voltage and low power LNA design integrated in a TSMC 0.18 μm CMOS process, and its sensitivity analysis. This sensitivity analysis gives a measure of the sensitivity of the LNA performance to a change in the circuit element values, thereby assisting the designer in choosing the adequate circuit element tolerances. Such sensitivity analysis of the LNA is very beneficial for making appropriate design trade offs. The designed LNA requires only a 1 V supply voltage and consumes 4.5 mW DC power. At 5.8 GHz, this LNA has noise figure (NF) of 2.463 dB, with input return loss of -15.35 dB, output return loss of -16.26 dB, and voltage gain of 11.57 dB.

5.1 Introduction

The first stage of a receiver is typically a low noise amplifier (LNA), whose main function is to provide enough gain to overcome the noise of subsequent stages (such as mixer) [1]. In the literature, many LNA's are designed in GaAs and bipolar technology [9, 8]. As the cutoff frequency of CMOS device has increased above a few tens of GHz, CMOS circuits are capable of replacing GaAs/bipolar circuits in the area of a few-GHz RF. Since CMOS technology has the feature of low cost, high level of integration, and mass productivity, it becomes very popular in RF integrated circuit design currently [7].

Much research has been done in the CMOS LNA area from 900 MHz to 2.4 GHz [5, 3, 2, 1, 4]. As the demand for Radio Frequency Integrated Circuits operating at higher frequency bands increases, circuit design in an IEEE 802.11a standard becomes

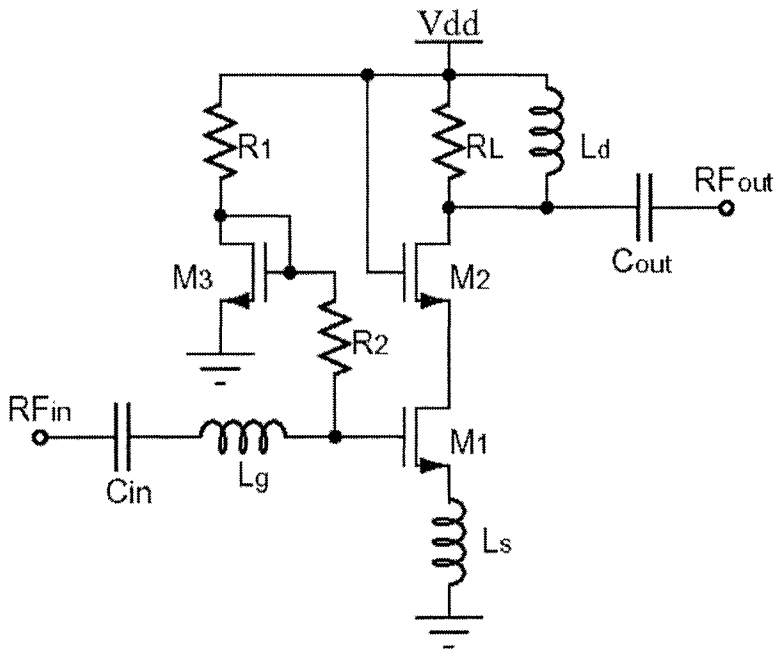

Figure 5.1 Complete schematic of the 5.8 GHz LNA

a very interesting area. However, there are fewer examples of CMOS LNA designed at 5-6 GHz.

In this paper, a low voltage and low power CMOS LNA at 5.8GHz is proposed. As a design tool, sensitivity analysis gives a measure of sensitivity of the LNA circuit performance to a change in the circuit element values,thereby assisting the designer in choosing adequate circuit-element tolerances. Such sensitivity analysis of the LNA is very beneficial for making appropriate design trade offs. In this paper, the sensitivity analysis of the proposed LNA circuit is also provided.

The remainder of this paper is organized as follows: In the next section, a single-ended 5.8 GHz RF CMOS LNA circuit design is proposed. Section 6.3 shows the simulation results. Section 5.4 describes the sensitivity analysis of the proposed LNA design. Finally, some conclusions are given in Section 6.4.

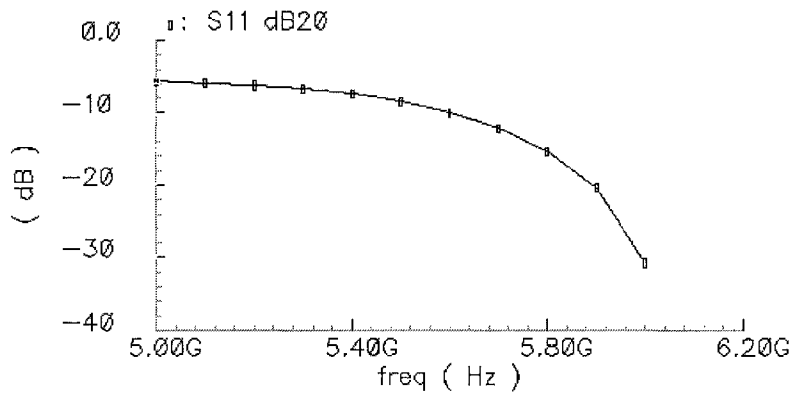

Figure 5.2 LNA s11

5.2 LNA Circuit Design

The complete schematic of the 5.8 GHz LNA is shown in Figure 5.1, where L_g, L_s, and L_d are all implemented with on-chip spiral inductors. The method employed here is inductive source degeneration. Cascoding transistor M_2 is used to reduce the interaction of the tuned output with the tuned input, and to reduce the effect of the gate-drain capacitance C_{gd} of M_1. The inductors L_g and L_s are chosen to provide the desired input resistance. L_d and the capacitance of the transistors M_2 form a tank circuit to tune the LNA to 5.8GHz. M_3, R_1, and R_2 form a bias circuit. Transistor M_3 essentially forms a current mirror with M_1, where its width is a small fraction of the width of M_1's in order to minimize the power overhead of the bias circuit. C_{in} and C_{out} are DC blocking capacitors.

Due to the limited choice of inductor and capacitor values in the technology we choose, the matching network becomes very challenging. With the comprehensive consideration of the chip size and different performance tradeoff, C_{in} and C_{out} play important roles in input and output matching respectively. The load resistor R_L is tuned to manage the tradeoff between gain, output matching, and power dissipation of LNA. Both input and output are matched to 50 Ω.

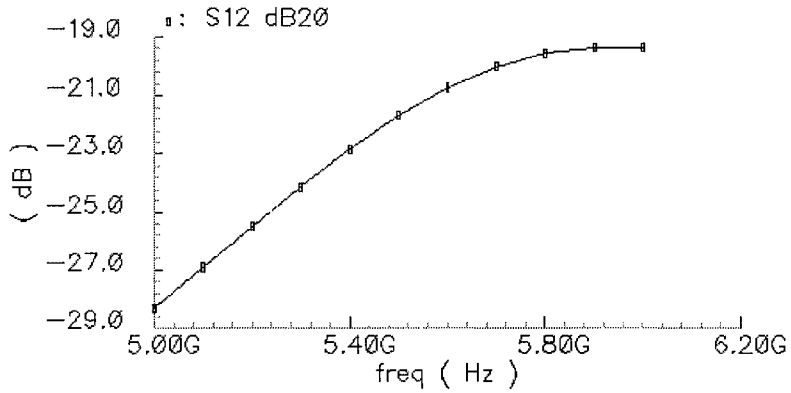

Figure 5.3 LNA s12

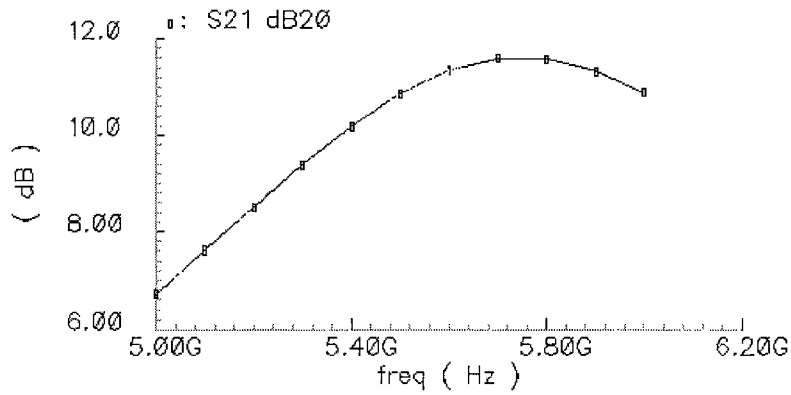

Figure 5.4 LNA s21

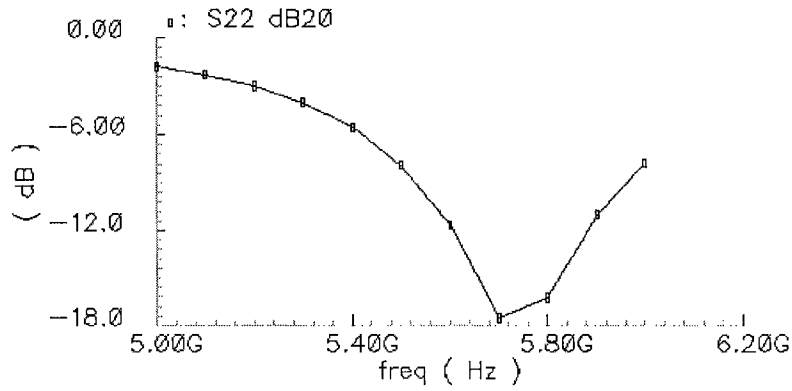

Figure 5.5 LNA s22

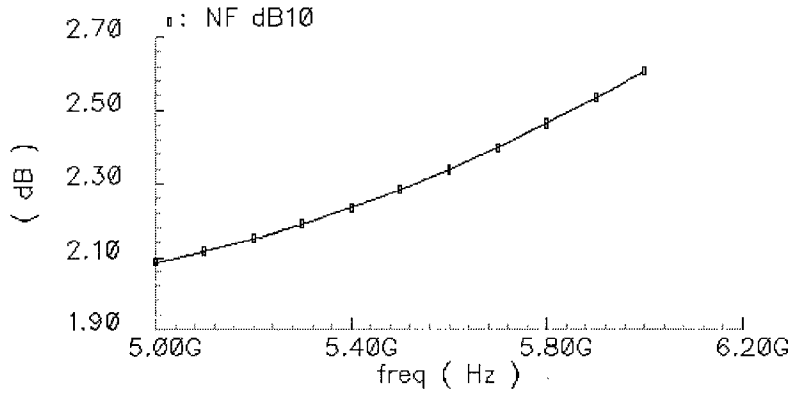

Figure 5.6 LNA noise figure

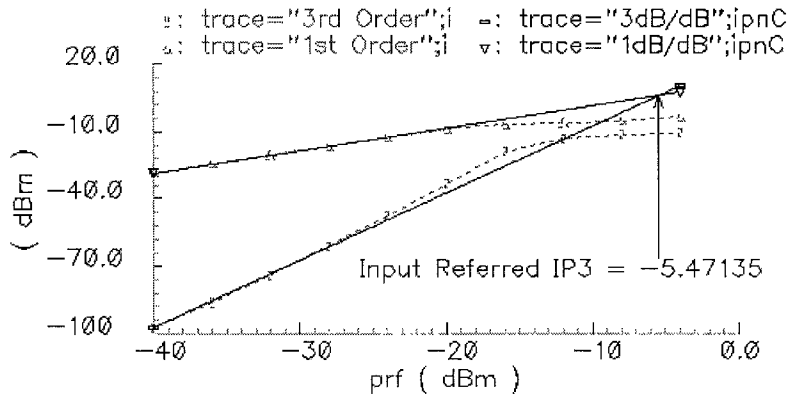

Figure 5.7 LNA IIP3

Table 5.1 Performance summary of the LNA

Parameter	Value
Technology	0.18 μm CMOS
Frequency	5.8 GHz
Gain	11.57 dB
NF	2.463 dB
S_{11}	-15.35 dB
S_{22}	-16.26 dB
S_{12}	-19.56 dB
IIP3	-5.47dBm
Supply Voltage	1 V
Power Dissipation	4.5 mW

Table 5.2 Comparison to other low voltage CMOS LNA's operation above 5 GHz

	This Work	[1]
Technology	0.18 μm CMOS	
Frequency	5.8 GHz	
Supply Voltage	1 V	
Power Dissipation	4.5 mW	22.2 mW
Gain	11.57 dB	13.2 dB
NF	2.463 dB	2.5 dB
S_{11}	-15.35 dB	-5.3 dB
S_{22}	-16.26 dB	-10.3 dB

5.3 Simulation Results

For the proposed single-ended LNA shown in Figure 5.1, the simulation result is shown in Figure 5.2–Figure 5.7. The designed LNA requires only a 1 V supply voltage and consumes 4.5 mW power. At 5.8 GHz, this LNA has noise figure (NF) of 2.463 dB, with input return loss of -15.35 dB, output return loss of -16.26 dB, and voltage gain of 11.57 dB. This LNA performance represents high voltage gain, low supply voltage, low noise figure, and low power dissipation. The performance summary is listed in Table 6.1.

Table 5.2 lists the comparison to another low voltage CMOS LNA's operation above

5 GHz. Note that [1] represents the experimental results.

5.4 LNA Sensitivity Analysis

In this section, sensitivity analysis of the proposal LNA is described. We mainly focus on the sensitivity analysis of gain and noise figure to the inductors. Suppose we are interested in the sensitivity of the gain to L_g, L_s, and L_d. We choose the same variation for L_g, L_s, and L_d, then we calculate $\Delta L/L$, and Δgain/gain. Note that gain is in an absolute value, not in dB.

The overall stage transconductance G_m is

$$G_m = g_{m1}Q_{in} = \frac{g_{m1}}{\omega_0 C_{gs}(R_s + \omega_T L_s)} \tag{5.1}$$

where

$$\omega_0 = \frac{1}{\sqrt{(L_g) + L_s C_{gs}}} \tag{5.2}$$

The gain of LNA is

$$A_v = G_m Z_L. \tag{5.3}$$

It shows that the gain is determined by transistor size, L_g, L_s, and load impedance Z_L.

The gain, noise figure, and the third order input intercept point (IIP3) variation versus L_g, L_s, and L_d variation are shown in Figure 5.8–Figure 5.10.

From Figure 5.8 and Figure 5.10, we can see that both the gain and IIP3 are more sensitive to the change in L_d compared to L_g and L_s. They also indicate that both the gain and IIP3 are more sensitive to the change in L_s than L_g.

From Figure 5.9, we can see that the noise figure is more sensitive to the change in L_s and L_g than L_d. And it shows that the noise figure is more sensitive to the change in L_s than L_g.

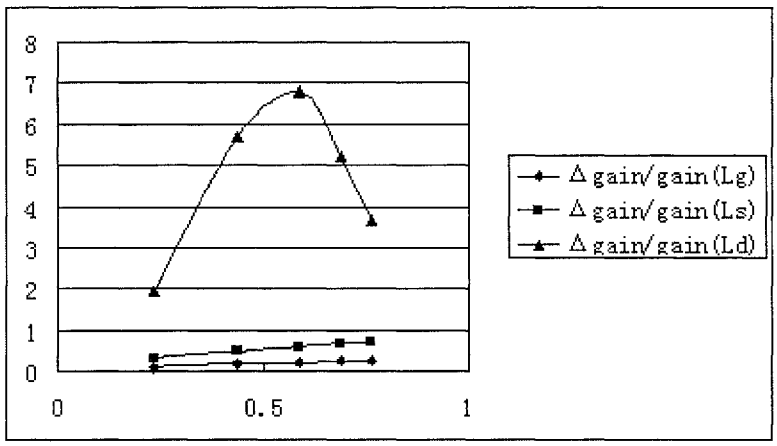

Figure 5.8 LNA gain variation versus L_g, L_s, and L_d variation

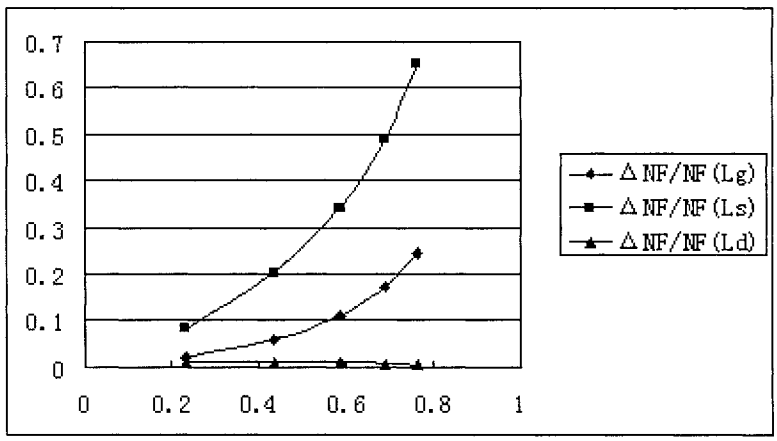

Figure 5.9 LNA noise figure variation versus L_g, L_s, and L_d variation

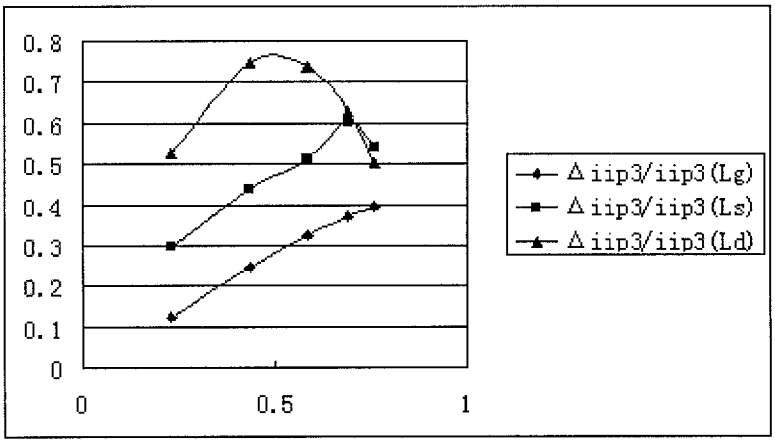

Figure 5.10 LNA iip3 versus L_g, L_s, and L_d variation

5.5 Conclusions

This paper presents a 5.8 GHz LNA design integrated in a TSMC 0.18 μm CMOS process, and its sensitivity analysis. Such sensitivity analysis of the LNA provides some insights of the proposed LNA design. The designed LNA requires only a 1 V supply voltage and consumes 4.5 mW power. At 5.8 GHz, this LNA has noise figure (NF) of 2.463 dB, with input return loss of -15.35 dB, output return loss of -16.26 dB, and voltage gain of 11.57 dB. This LNA performance represents high voltage gain, low supply voltage, low noise figure, and low power dissipation. This LNA can be used for low voltage and low power wireless applications. Future work may be focused on LNA optimization analysis based on the results of the sensitivity analysis.

Bibliography

[1] T. Tsang and M. El-Gamal, "Gain and frequency controllable sub-1V 5.8 GHz CMOS LNA" *2002 IEEE International Symposium on Circuits and Systems*, vol. 4, pp. 795-798, 2002.

[2] A. Parssinen, S. Lindfors, J. Ryynanen, S. Long, and K. Halonen, "1.8 GHz CMOS LNA with on-chip DC-coupling for a subsampling direct," *1998 IEEE International Symposium on Circuits and Systems*, pp. 73-76, 1998.

[3] H. Jin and C. Salama, "A 1-V 1.9-GHz CDMA CMOS on SOI low noise amplifier," *2000 IEEE International SOI Conference*, pp. 102-103, 2000.

[4] R. Point, M. Mendes, and W. Foley, "A differential 2.4 GHz switched-gain cmos lna for 802.11b and bluetooth," *2002 IEEE Radio and Wireless Conference*, pp. 221-224, 2002.

[5] E. Sacchi, I. Bietti, F. Gatta, F. Svelto, R. Castello, "Nonlinear inversion-based output tracking," *A 2 dB NF fully differential variable gain 900 MHz CMOS LNA*, pp. 94-97, 2000.

[6] T. Lee, *The Design of CMOS Radio-Frequency Integrated Circuits*, Cambridge University Press, 1998.

[7] S. Park and W. Kim "Design of a 1.8 GHz low-noise amplifier for RF front-end in a 0.8," *IEEE Transactions on Consumer Electronics*, vol. 47, pp. 10-15, 2001.

[8] B. Ray, T. Manku, R. Beards, J. Nisbet, and W. Kung, "A highly linear bipolar 1 V folded cascode 1.9 GHz low noise," *Proceedings of the 1999 Bipolar/BiCMOS Circuits and Technology Meeting*, pp. 157-160, 1999.

[9] H. Morkner, M. Frank, and B. Ingram, "A novel 3 V 7 mA PHEMT GaAs active MMIC mixer/LNA for wireless," *1995 Microwave Systems Conference*, pp. 29-32, 1995.

[10] R. Rafla, and M. El-Gamal, "2.4-5.8 GHz CMOS LNA's using integrated inductors," *Proceedings of the 43rd IEEE Midwest Symposium on Circuits and Systems*, vol. 1, pp. 302-304, 2000.

6 A Novel 1.5V CMFB CMOS Down-Conversion Mixer Design for IEEE 802.11a WLAN Systems

Abstract — This paper presents a 5.8 GHz low voltage down-conversion mixer design integrated in a TSMC 0.18 μm CMOS process. The proposed method features that an RF input stage converts the RF input voltage to current, which is coupled to the core of a Gilbert Cell using a current mirror. This implementation eliminates the current source transistor at the bottom and furthermore reduces the supply voltage. Common-mode feedback is used for the active load of the mixer. The LO frequency is at 5.6 GHz. The designed mixer requires only a 1.5 V supply voltage and consumes 11.78 mW DC power. At 5.8 GHz, this mixer has a single-sideband noise figure (SSB NF) of 13.6 dB, with an input return loss of -18 dB, with an output return loss of -26.4 dB, a Third-order Input Intercept Point (IIP3) of -10.66 dBm, and conversion gain of 10.4 dB.

6.1 Introduction

Wireless communications research has experienced a remarkable renaissance in the last decade. The growing wireless LAN market has generated increasing interest in technologies that will enable higher data rates and capacity than initially deployed systems. The 802.11b standard at the 2.4 GHz ISM band provides data rates up to 11Mbps with direct sequence spread spectrum (DSSS). This technology first appeared in the market in 1999. The 802.11a standard, released by IEEE in 1999, is based on an orthogonal frequency division multiplexing (OFDM) modulation technology with data rates up to 54 Mbps in the 5GHz band [3]. The IEEE 802.11a standard provides nearly five times the data rate and as much as ten times the overall system capacity as currently available

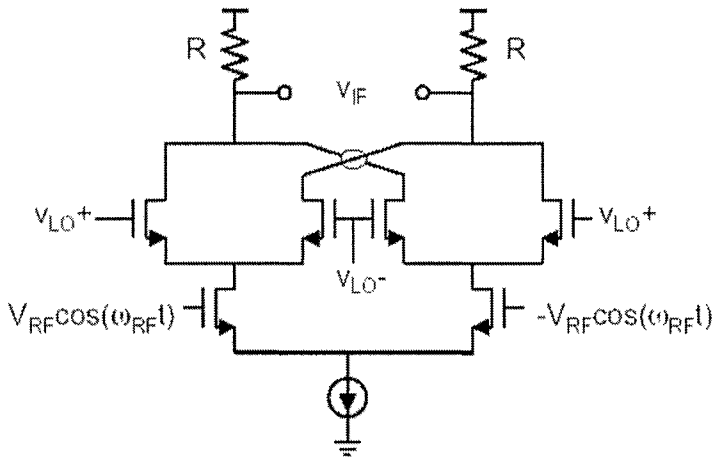

Figure 6.1 MOS version of Gilbert-type mixer

802.11b wireless LAN systems [5]. Fast growth of the personal communication market requires low cost production and low power transceivers for wireless applications. As a low cost alternative, CMOS is becoming a contender for RF front-end IC applications [6].

In low-voltage RF IC design, high LO drives are difficult to generate. The down-conversion mixer translates an incoming RF signal to a lower frequency, known as the intermediate frequency (IF) [1]. Both in bipolar and CMOS technologies, down-conversion mixers have good gain and linearity [11, 12].

The most common mixer architecture is a Gilbert-cell [7]. The MOS version of the Gilbert-type mixer is shown in Figure 6.1. However, it cannot operate at near 1 V supply due to the stack of three saturated transistors. Thus designing a CMOS mixer that can operate at 5-6 GHz with low voltage becomes a challenging task.

Among the CMOS mixer research areas, some works have been done in targeting low voltage mixer design. Cheng *et al.* designed a 1.2 V, 900 MHz CMOS mixer circuit using current mode multiplication method [9]. However, the conversion gain is only -9 dB. Kathiresan *et al.* proposed a CMOS mixer core, operating at 1GHz, where the RF signal is input via the bulk [10]. But their conversion gain is only 2.09 dB.

Due to the limitations of the existing research work, Wang *et al.* proposed a low-

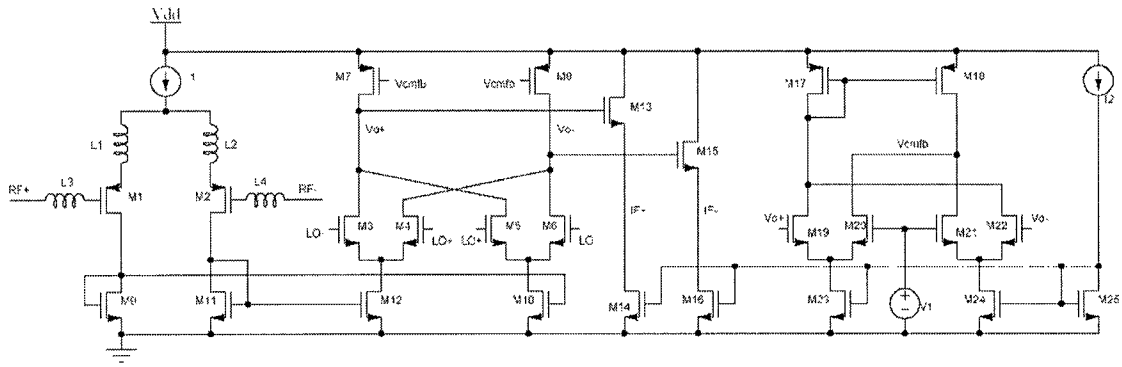

Figure 6.2 Complete schematic of the 5.8 GHz mixer with common mode feedback structure

voltage 5.8 GHz mixer design in a TSMC 0.18 m CMOS process [2]. This paper is a further improvement of the design in [2].

This paper presents a novel 1.5 V 5.8 GHz mixer design integrated in a TSMC 0.18 m CMOS process. The remainder of this paper is organized as follows: In the next section, a single-ended 5.8 GHz RF CMOS mixer circuit design is proposed. Section 6.3 shows the simulation results. Finally, some conclusions are given in Section 6.4.

6.2 Mixer Circuit Design

The complete schematic of the proposed 5.8 GHz mixer is shown in Figure 6.2.

Compared to the traditional Gilbert Cell architecture, this method features that the PMOS transistors $M1$ and $M2$ are used for the RF input stage to convert the RF input voltage to current, which is coupled to the core of Gilbert Cell using current mirror (transistors $M_9 - M_{10}$ and $M_{11} - M_{12}$). This implementation eliminates the current source transistor at bottom and furthermore reduces the supply voltage.

The inductors $L_1 - L_4$ are all implemented with on-chip spiral inductors. The source degeneration inductors L_1 and L_2, combined with gate inductors L_3 and L_4, are for the input matching. The RF input is matched to 50 Ω. The source degeneration structure helps to decrease the noise figure and increase the IIP3. The downside of on-chip matching is that it consumes a larger chip size.

PMOS transistors M_7 and M_8 are the loads of the mixer. The DC current flows through the PMOS transistors M_7 and M_8.

Compared to the design in [2], the proposed design has a common-mode feedback (CMFB) structure. In Figure 6.2, transistors $M17$ - $M24$ form a CMFB circuit. It fixes the common-mode voltage of Vo+ and Vo- around 1.1 V. Such a structure guarantees that there is only a V_{ds} voltage drop from V_{dd} which make the circuit work at a low voltage condition and also enlarges the output swing at the same time.

Transistors $M_{13} - M_{16}$ compose a source follower. The mixer IF output is taken from the sources of NMOS transistors M_{13} and M_{15}. The source follower increases the output driving capacity and matches the output to 50 Ω at the IF frequency.

At the same time, it is valuable to point out that even though such PMOS pull-up current sources can operate with lower headroom, they may suffer from large flick noise [8].

In our paper, the RF frequency is at 5.8 GHz and the LO frequency is at 5.6 GHz. The IF Frequency is at 200 MHz. The flicker noise is relatively low at 200 MHz. Therefore, such a structure doesn't affect the noise figure performance. However, for a low IF application, flicker noise may come into the picture. Based on the corresponding noise figure requirements, the proposed structure may need to be adjusted.

6.3 Simulation Results

The proposed mixer shown in Figure 6.2 is simulated in a TSMC 0.18 μm CMOS process using a Cadence 446 Specture-RF simulator. The simulation results are shown in Figure 6.3–Figure 6.7. The designed mixer requires only a 1.5 V supply voltage and consumes 11.78 mW power. At 5.8 GHz, this mixer has a single-side band noise figure (SSB NF) of 13.6 dB, with an input return loss of -18 dB, an IIP3 of -10.66 dBm, and a conversion gain of 10.4 dB. The performance summary is listed in Table 6.1.

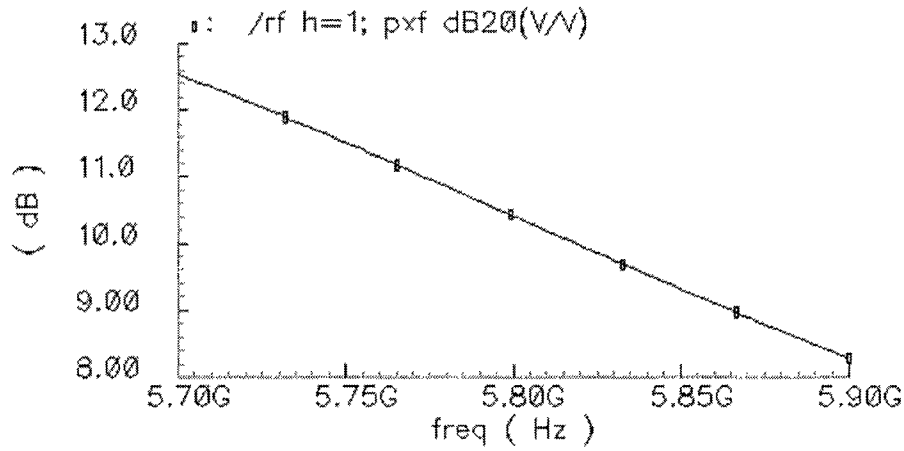

Figure 6.3 Conversion gain of the mixer

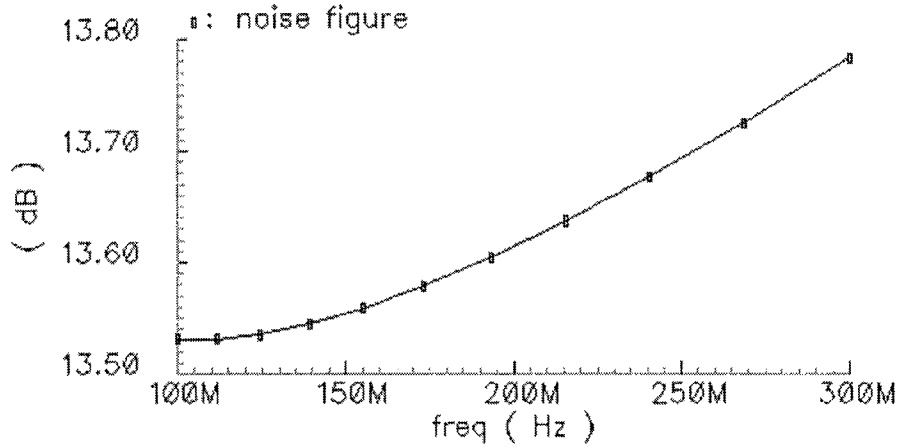

Figure 6.4 Noise figure of the mixer

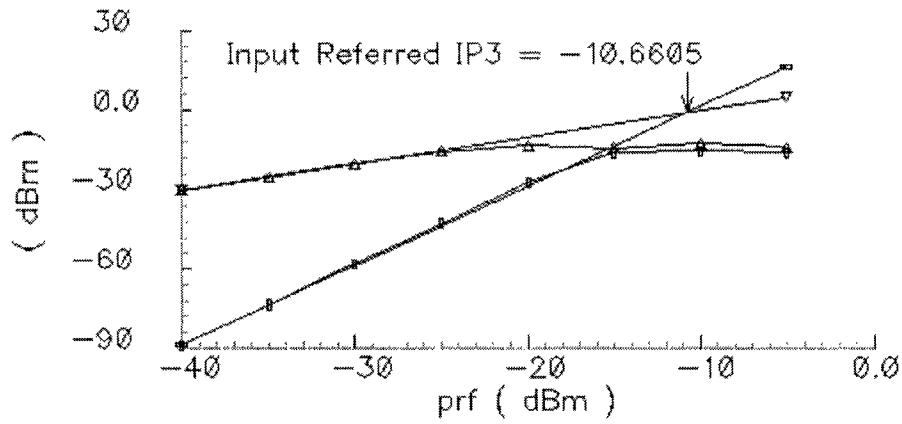

Figure 6.5 IIP3 of the mixer

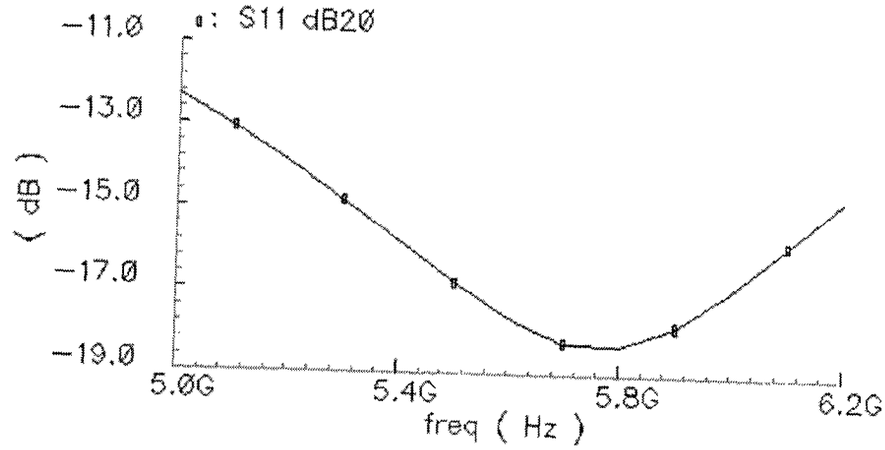

Figure 6.6 S_{11} of the mixer

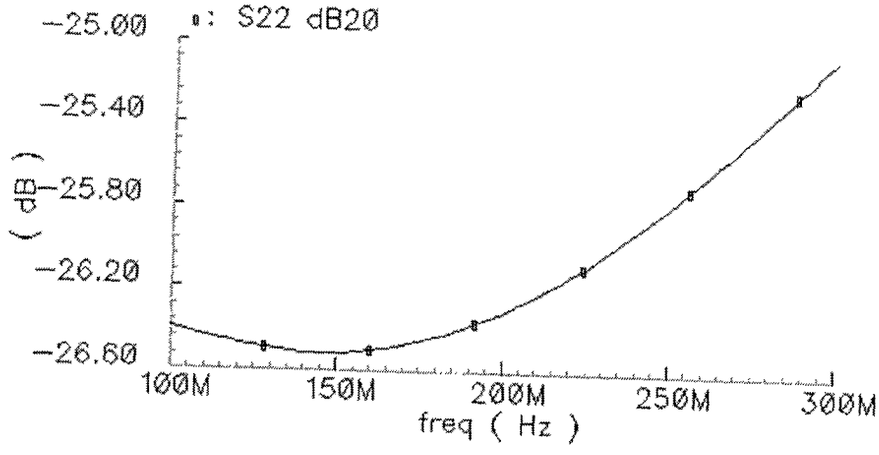

Figure 6.7 S_{22} of the mixer

Table 6.1 Performance summary of the mixer

Parameter	Value
Technology	0.18 μm CMOS
Supply Voltage	1.5 V
Power Dissipation	11.78 mW
RF Frequency	5.8 GHz
LO Frequency	5.6 GHz
IF Frequency	200 MHz
Conversion Gain	10.4 dB
SSB Noise Figure	13.6 dB
IIP3	-10.66 dBm
S_{11}	-18 dB
S_{22}	-26.4 dB

6.4 Conclusions

This paper has described a low-voltage 5.8 GHz mixer design integrated in a TSMC 0.18 μm CMOS process. The proposed method features an RF input stage that converts the RF input voltage to current, which is coupled to the core of Gilbert Cell using a current mirror. This implementation eliminates the current source transistor at the bottom and furthermore reduces the supply voltage. Common-mode feedback is used for the active load of the mixer. The designed mixer requires only a 1.5 V supply voltage and consumes 11.78 mW power. At 5.8 GHz, this mixer has noise figure (NF) of 14.3 dB, with an input return loss of -18 dB, with an output return loss of -26.4 dB, an IIP3 of -10.66 dBm, and a conversion gain of 10.4 dB. This mixer can be used for low voltage and low power wireless applications. For future research, sensitivity analysis optimization of the proposed mixer will be interesting to study.

Bibliography

[1] T. Lee, *The Design of CMOS Radio-Frequency Integrated Circuits*, Cambridge University Press, 1998.

[2] X. Wang and R. Weber, "A novel low-voltage low-power 5.8 GHz CMOS down-conversion mixer design" *2003 IEEE Radio and Wireless Conference*, pp. 301-304, 2003.

[3] B. Klepser, M. Punzenberger, T. Ruhlicke, and M. Zannoth, "5-GHz and 2.4-GHz dual-band RF-transceiver for WLAN 802.11a/b/g applications," *2003 IEEE Radio Frequency Integrated Circuits (RFIC) Symposium*, pp. 37-40, 2003.

[4] C. Pavoluta, C. Neacsu, M. Derevlean, and G. Arsinte, "CMOS RF mixer design - A noise cancellation approach," *2003 International Symposium on Signals, Circuits and Systems*, vol. 1, pp. 245-248, 2003.

[5] M. Zargari, D. Su, C. Yue, S. Rabii, D. Weber, B. Kaczynski, S. Mehta, K. Singh, S. Mendis, B. Wooley, "A 5-GHz CMOS transceiver for IEEE 802.11a wireless LAN systems," *IEEE Journal of Solid-State Circuits*, vol. 37, pp. 1688-1694, 2002.

[6] T. Manku, "Microwave CMOS-device physics and design," *IEEE Journal of Solid-State Circuits*, vol. 34, pp. 277-285, 1999.

[7] B. Gilbert, "A precise four-quadrant multiplier with subnanosecond responsen," *IEEE Journal of Solid-State Circuits*, vol. 3, pp. 365-373, 1968.

[8] H. Sjoland, A. Karimi-Sanjaani, and A. Abidi, "A merged CMOS LNA and mixer for a WCDMA receiver," *IEEE Journal of Solid-State Circuits*, vol. 38, pp. 1045-1050, 2003.

[9] W. Cheng, C. Chan, C. Choy, and K. Pun, "A 1.2 V 900 MHz CMOS mixer," *Proceedings of the IEEE International Symposium on Circuits and Systems*, vol. 5, pp. 365-368, 2002.

[10] G. Kathiresan and C. Toumazou, "A low voltage bulk driven downconversion mixer core," *Proceedings of the IEEE International Symposium on Circuits and Systems*, vol. 2, pp. 598-601, 1999.

[11] B. Rezavi, "A 1.5 V 900 MHz downconversion mixer," *IEEE International Solid-State Circuits Conference Digest of Technical Papers*, pp. 48-49, 1996.

[12] J. Crols and M. Steyaert, "A single-chip 900 MHz CMOS receiver front-end with a high," *IEEE Journal of Solid-State Circuits*, vol. 30, pp. 1483-1492, 1995.

7 CONCLUSIONS AND FUTURE RESEARCH

7.1 Conclusions

This thesis is composed of two parts. The first part of the thesis has addressed the inversion-based output tracking control and learning control for nonminimum phase systems, which contained chapter 2 to chapter 4. The second part of the thesis has presented low voltage and low power RF CMOS LNA and mixer design, which included chapter 5 and chapter 6.

In Chapter 2, we have introduced a new procedure for designing a nonminimum phase output tracking controller driven by a causal reference profile. In this approach, the nonminimum phase system is first stably inverted on-line to obtain both desired (and stable) state and input trajectories. Then an H_∞ optimal controller is used to stabilize the closed-loop system. We provide a causal inversion solution for general nonlinear systems. By using the scaling property, we present a causal inversion solution such that the causal state and input trajectories track those obtained by stable inversion approach for linear systems. This new controller has achieved stable $\epsilon-$tracking. In contrast to stable inversion, the causal inversion approach does not require precalculation. In contrast to nonlinear regulation, the causal inversion approach avoids the numerical intractability of solving nonlinear PDEs. This causal inversion-based controller has been applied to a tip trajectory tracking of a one-link flexible manipulator. Simulation results demonstrate that the causal inversion approach is very effective for obtaining output tracking for flexible manipulators. This new approach has many important engineering applications such as in rocket tracking and aircraft altitude control problems.

In Chapter 3, a new adaptive learning algorithm has been developed for unstable

nonminimum systems. The adaptive backstepping feedback control law is employed to guarantee regulation of tracking error and a stable inverse system is used to update the feed forward input for the next trial. We have shown that, given a desired trajectory, the learning controller is able to learn and eventually drive the closed loop dynamics to track the desired trajectory.

In Chapter 4, a sufficient condition for the convergence of the proposed inversion-based robust learning algorithm has been provided. We have shown that simulation studies on two types of linear systems with gain uncertainty and time constant uncertainty are presented. The simulation results have demonstrated the effectiveness of the proposed method.

Chapter 5 presented a 5.8 GHz LNA design integrated in a TSMC 0.18 μm CMOS process and its sensitivity analysis. This LNA performance has represented high voltage gain, low supply voltage, low noise figure, and low power dissipation.

Finally, Chapter 6 has described a novel low-voltage 5.8 GHz mixer design with a common-mode feedback structure. It has been integrated in a TSMC 0.18 μm CMOS process. The performance of the designed mixer has been discussed.

Both LNA and mixer design approaches can be used for low voltage and low power wireless applications.

7.2 Future Research

Future research issues related to the area addressed in this thesis may include the following:

1. Reference output trajectories. Can the causal inversion approach allow more general reference output trajectories?

2. Convergence condition. What is the convergence condition for the inversion-based adaptive learning algorithm?

3. Nonlinear systems. How to extend the inversion-based robust learning algorithm to nonlinear systems?

4. Optimization study. How to do an optimization design for a LNA? Can the results of the sensitivity analysis help in the LNA optimization design?

5. Challenges for low voltage RF CMOS receiver design. What are the structures for other blocks in a low voltage RF CMOS receiver, such as a voltage gain amplifier (VGA), voltage controlled oscillator (VCO), and a high gain op amp?